Acta Pharmaceutica Sinica B 2022;12(6):2887–2904

Chinese Pharmaceutical Association
Institute of Materia Medica, Chinese Academy of Medical Sciences

Acta Pharmaceutica Sinica B

www.elsevier.com/locate/apsb
www.sciencedirect.com

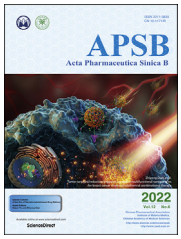

ORIGINAL ARTICLE

Gentiopicroside targets PAQR3 to activate the PI3K/AKT signaling pathway and ameliorate disordered glucose and lipid metabolism

Haiming Xiao[a,c,†], Xiaohong Sun[a,†], Zeyuan Lin[a,†], Yan Yang[a], Meng Zhang[a,c], Zhanchi Xu[b], Peiqing Liu[a,c,*], Zhongqiu Liu[b,*], Heqing Huang[a,c,*]

[a]*Laboratory of Pharmacology & Toxicology, School of Pharmaceutical Sciences, Sun Yat-sen University, Guangzhou 510006, China*
[b]*School of Pharmaceutical Sciences, Guangzhou University of Chinese Medicine, Guangzhou 510006, China*
[c]*National and Local United Engineering Lab of Druggability and New Drugs Evaluation, School of Pharmaceutical Sciences, Sun Yat-sen University, Guangzhou 510006, China*

Received 18 September 2021; received in revised form 8 November 2021; accepted 10 November 2021

KEY WORDS

Gentiopicroside;
Insulin resistance;
PAQR3;
PI3K/AKT;
DDB2;
Ubiquitylation;
Glucose metabolism disorder;
Lipid metabolism disorder

Abstract The obstruction of post-insulin receptor signaling is the main mechanism of insulin-resistant diabetes. Progestin and adipoQ receptor 3 (PAQR3), a key regulator of inflammation and metabolism, can negatively regulate the PI3K/AKT signaling pathway. Here, we report that gentiopicroside (GPS), the main bioactive secoiridoid glycoside of *Gentiana manshurica Kitagawa*, decreased lipid synthesis and increased glucose utilization in palmitic acid (PA) treated HepG2 cells. Additionally, GPS improved glycolipid metabolism in streptozotocin (STZ) treated high-fat diet (HFD)-induced diabetic mice. Our findings revealed that GPS promoted the activation of the PI3K/AKT axis by facilitating DNA-binding protein 2 (DDB2)-mediated PAQR3 ubiquitinated degradation. Moreover, results of surface plasmon resonance (SPR), microscale thermophoresis (MST) and thermal shift assay (TSA) indicated that GPS directly binds to PAQR3. Results of molecular docking and cellular thermal shift assay (CETSA) revealed that GPS directly bound to the amino acids of the PAQR3 NH_2-terminus including Leu40, Asp42, Glu69, Tyr125 and Ser129, and spatially inhibited the interaction between PAQR3 and the PI3K catalytic subunit (P110α) to restore the PI3K/AKT signaling pathway. In summary, our study identified GPS, which inhibits PAQR3 expression and directly targets PAQR3 to restore insulin signaling pathway, as a potential drug candidate for the treatment of diabetes.

*Corresponding authors.
E-mail addresses: liupq@mail.sysu.edu.cn (Peiqing Liu), liuzq@gzucm.edu.cn (Zhongqiu Liu), huangheq@mail.sysu.edu.cn (Heqing Huang).
†These authors made equal contributions to this work.
Peer review under responsibility of Chinese Pharmaceutical Association and Institute of Materia Medica, Chinese Academy of Medical Sciences.

https://doi.org/10.1016/j.apsb.2021.12.023
2211-3835 © 2022 Chinese Pharmaceutical Association and Institute of Materia Medica, Chinese Academy of Medical Sciences. Production and hosting by Elsevier B.V. This is an open access article under the CC BY-NC-ND license (http://creativecommons.org/licenses/by-nc-nd/4.0/).

© 2022 Chinese Pharmaceutical Association and Institute of Materia Medica, Chinese Academy of Medical Sciences. Production and hosting by Elsevier B.V. This is an open access article under the CC BY-NC-ND license (http://creativecommons.org/licenses/by-nc-nd/4.0/).

1. Introduction

Type 2 diabetes mellitus (T2DM) is characterized by a lipid and glucose metabolism disorder in which the clinical manifestations are mainly insulin resistance and relative insulin deficiency[1,2]. Under physiological conditions, insulin activates a hepatic insulin signaling pathway to increase hepatic glycogen storage and inhibit hepatic gluconeogenesis, and also regulates lipid synthesis, which is the most important mechanism to maintain glucose and lipid metabolism homeostasis[3]. It is well recognized that hepatic insulin resistance (HIR) is a key factor in the development of metabolic diseases such as T2DM and non-alcoholic fatty liver disease (NAFLD)[4,5]. The global epidemic of NAFLD affects more than 55% of individuals with type II diabetes[6] and the prevalence of non-alcoholic steatohepatitis (NASH) has been estimated to be 37% in type II diabetic patients[7]. This has focused attention on the liver as a main target to combat metabolic disorders as well as type II diabetes.

Generally, post-insulin receptor blocking refers to the insulin signal obstruction that leads to insulin resistance, which is the main pathology of clinical insulin-resistant diabetes[8]. As the central link in the insulin pathway, the PI3K/AKT axis regulates hepatic glycogen synthesis, gluconeogenesis and lipid synthesis[9,10]. An activated PI3K/AKT axis regulates GSK-3β kinase activity and FOXO1 transcription to increase GCK activity and reduce G6Pase expression, thereby promoting hepatic glycogen synthesis and gluconeogenesis[11,12]. Moreover, the PI3K/AKT axis regulates lipogenesis by inhibiting sterol regulatory element binding transcription factor (SREBP-1c), subsequently increasing hepatic LDLR protein expression[13]. New drugs that are in the pipeline and older drugs already approved for type II diabetes have focused on improving PI3K/AKT axis transduction[14−16]. Phosphoinositide 3-kinase (PI3K) mediates insulin actions by transferring signals from insulin receptors (INSRs) to downstream targets. Class IA PI3K contains heterodimers of a p110 catalytic subunit (p110α, p110β, and p110δ) and a p85 regulatory subunit (p85α, p85β, and p55γ)[17]. The p110α catalytic subunit of class IA PI3K is the primary insulin-responsive PI3K and the p110α−p85α complex is the PI3K heterodimer implicated in insulin signaling[18,19]. Therefore, facilitating the formation of p110α−p85α dimer is a promising strategy to improve insulin sensitivity of cells.

Progestin and adipoQ receptor 3 (PAQR3, also known as RKTG) is a seven transmembrane receptor located on the Golgi membrane, which is a member of the PAQR protein family[20]. PAQR3 is widely distributed in a variety of tissues, and is highly expressed in skin, liver, kidney and testis tissues[21]. The PAQR3 signaling pathway is involved in a variety of physiological and pathological processes, and has a clear role in promoting inflammation[22−24]. Recently, the role of PAQR3 in regulating glucose and lipid metabolism has been emphasized[22,25]. Previous studies have shown that the aberrant up-regulation of PAQR3 activates the NF-κB signaling pathway, thereby promoting renal fibrosis and hepatic insulin resistance[23,24]. Additionally, it has been reported that PAQR3 knockout significantly improved diabetic fatty liver, insulin resistance and energy utilization in HFD-induce mice[26]. Moreover, other studies have shown that PAQR3 promoted the formation of PCSK9 and LDLR complexes, and subsequently increase LDLR degradation *via* a lysosomal pathway to aggravate the accumulation of cholesterol[27]. Importantly, as an upstream regulator of the PI3K/AKT pathway, PAQR3 was found to negatively regulate insulin signaling by shunting cytosolic p110α to the Golgi apparatus while competing with the p85α subunit in formation of a PI3K complex with p110α[28]. This makes PAQR3 a promising target to combat insulin resistance. DDB2 (damage-specific DNA-binding protein 2) is the product of the xeroderma pigmentosum group E gene which is involved in the initiation of molecular ubiquitination *via* a ubiquitin ligase complex together with DDB1 and CUL4A (cullin 4A)[29−31]. Recently, DDB2 has been identified as a post-translational regulator of PAQR3, which can directly bind to PAQR3 to promote the ubiquitination of PAQR3 and restore insulin signal[32]. Therefore, inhibiting PAQR3 protein expression *via* DDB2-mediated ubiquitin degradation will contribute to the prevention of PI3K/AKT axis obstruction.

Gentiopicroside (Supporting Information Fig. S1A) is the main active compound of *Gentiana manshurica* Kitagawa with extensive pharmacological activities including anti-inflammatory, antioxidative and choleretic[33−35]. Recently, it was found that gentiopicroside ameliorated peripheral neuropathy and retinopathy effectively in diabetic mice[36,37]. Moreover, our previous study found that GPS significantly improved blood glucose levels and effectively inhibited inflammation to alleviate renal microvascular lesion[38]. However, whether and how GPS ameliorates HFD-induced glycolipid metabolism remains largely unknown. The present study demonstrates that GPS administration effectively improves hepatic insulin resistance to improve glucose and lipid metabolism disorder by promoting PI3K/AKT axis activation in STZ-HFD-treated mice. Mechanically, GPS facilitated the interaction between PAQR3 and DDB2 to promote DDB2-mediated PAQR3 ubiquitin degradation. Furthermore, GPS directly bound to the N-terminus of PAQR3 and spatially inhibited the interaction of PAQR3 and P110α to maintain the PI3K/AKT signaling pathway. GPS is the first natural compound with direct PAQR3 binding and PI3K/AKT axis restorative properties demonstrated both *in vivo* and *in vitro*.

2. Materials and methods

2.1. Cell culture

HepG2 cells (ATCC, Rockville, MD, US) were cultured in high-glucose DMEM containing 25 mmol/L glucose and 10% (*v*/*v*) FBS in a humidified incubator containing 5% CO_2. After the cells reached about 50% confluence, culture was continued in serum-free DMEM for 12−16 h. Palmitate sodium was dissolved in 20% (*w*/*v*) BSA at 70 °C to obtain the palmitate solution. The PA/BSA solution was diluted with DMEM to the indicated concentration (0.25 mmol/L) before use. The control group was treated with 0.5% BSA. GPS was dissolved in dimethyl sulfoxide (DMSO, Sigma, USA) and diluted to the indicated concentration.

When protein phosphorylation was measured, the cells were stimulated with 100 nmol/L insulin for 10 min and then collected for Western blot.

2.2. Animal experiment

Male C57/BL6 mice (20 ± 2 g) aged 6−8 weeks were purchased from the Experimental Animal Center of Sun Yat-sen University (Guangzhou, China). All animals were kept in an SPF environment with alternating cycles of constant temperature and humidity, 12 h of light, and 12 h of darkness. All experimental operations are in compliance with the Chinese Animal Welfare Law and approved by the Ethics Committee of Sun Yat-sen University.

The diabetic mouse model was replicated as we previously reported[39]. Briefly, after male mice were adaptively fed for one week, they were fed with high-fat diet (high-fat diet, HFD containing 17% carbohydrates, 25% protein and 58% fat) for three weeks, and then injected intraperitoneally with STZ (40 mg/kg, dissolved in 0.1 mol/L citric acid buffer) for 5 days, and continued to be fed the HFD throughout the experiment. The mice that demonstrated polydipsia and polyuria with a fasting blood glucose (FBG) greater than 11.1 mmol/L were included in the diabetes model group. Forty diabetic mice were randomly divided into five groups as follows: (1) diabetes group (n = 8); (2) GPS treatment group (low dose: 25 mg/kg, n = 8); (3) GPS treatment group (medium dose: 50 mg/kg, n = 8); (4) GPS treatment group (high dose: 100 mg/kg, n = 8); and (5) metformin treatment group (195 mg/kg, n = 8). At the same time, the control group received normal feed and were injected with an equal volume of citrate buffer as a vehicle control. The gentiopicroside powder was dissolved to the indicated concentration with normal saline avoiding exposure to light, and the dosage selected was based on previous studies[34]. Gentiopicroside was given to the mice by intragastric administration, and the diabetic groups were given an equal volume of saline for 6 consecutive days every week. Liver and serum samples were obtained after the mice were killed, and the liver tissues were frozen in liquid nitrogen or embedded in paraffin. The graphic illustration of the animal experiment design is shown in Supporting Information Fig. S2.

2.3. Reagents and antibodies

GPS powder (HPLC purity > 99.0%) was obtained from Ronghe Science and Technology Ltd. (Shanghai, China) for cell experiments and biochemical assay. GPS powder (HPLC purity > 98.0%) was purchased from Zhenweikang Science and Technology Ltd. (Nanjing, China) for animal experiments. Fetal bovine serum (FBS) and Dualbecco's modified Eagle's medium (DMEM) were obtained from Gibco Invitrogen Corp. (Gibco, Carlsbad, CA, USA). Metformin (Catalog: S1741-1g, HPLC purity > 99%) was obtained from Beyotime (Nanjing, China). Metformin hydrochloride tablets used for animal experiments were purchased from Bristol Myers Squibb Co. (Shanghai, China). Streptomycin (STZ, Catalog: S0130) used in animal experiments, palmitate sodium (Catalog: P9767) and oil red O (Catalog: O0625) were obtained from Sigma−Aldrich Corp. (St. Louis, MO, USA). Bovine serum albumin (BSA, Catalog: A8850) was purchased from Solarbio (Beijing, China). A fluorescent D-glucose analog (2-NBDG, Catalog: N13195) was obtained from Invitrogen (Carlsbad, CA, USA). LY294002 (Catalog: T2008, HPLC purity > 99.0%) was purchased from Target Molecule Corp. (Boston, MA, USA). Rabbit IgG (Catalog: A7016), mouse IgG (Catalogue: A0216), methylthiazolyldiphenyl-tetrazolium bromide (MTT, Catalog: ST316), insulin (Catalog: P3376), His-labeled protein purification kit (Catalog: P2229S) and IPTG (catalog: ST098) were purchased from Beyotime (Haimen, China). The nuclear extract kit (Catalog: 40010) was purchased from Active Motif (Carlsbad, CA, USA) and the Golgi extract kit was obtained from Bestbio (Catalog: BB3604; Beijing, China). Antibodies are listed in Supporting Information Table S1. Alexa Fluor 647 donkey anti-mouse IgG, Alexa Fluor 594 donkey anti-rabbit IgG, Alexa Fluor 488 goat anti-mouse IgG and horse radish peroxidase were obtained from Thermo Fisher Scientific Inc. (Rockford, IL, USA). Other chemicals were purchased from Sigma−Aldrich unless specified otherwise and the chemicals are listed in Supporting Information Table S2.

2.4. Cell viability

HepG2 cells were treated with the indicated concentrations of GPS (5, 20, 40, 80, 160, and 320 μmol/L) for 24 h and then 0.5 mg/mL MTT was added to each well for another 4 h at 37 °C. The medium was discarded and 200 μL DMSO was added. Finally, the absorbance was detected by a microplate reader (Omega, Norwalk, CT, USA).

2.5. Cellular glucose uptake assay

After the HepG2 cells were treated with various stimuli, culture was continued with serum-free medium for another 3 h, and then the cells were treated with 50 μmol/L 2NBDG and 1 mmol/L insulin for 1 h. Finally, the cells were treated with trypsin for 3 min and the cell suspension was centrifuged for 3 min at 3000 rpm (PICO 17 centrifuge, ThermoFisher Scientific Inc., Rockford, IL, USA). The supernatant was removed and precooled PBS was added to resuspend the cells. The fluorescence intensity of 2NBDG was detected by flow cytometry at 488 nm.

2.6. Cellular oil red O staining and PAS staining

The oil red O powder was diluted with isopropanol to a concentration of 0.5% and then mixed with ultrapure water at a 3:2 ratio, and then filtered with 0.22 μm membrane. HepG2 cells were washed with PBS for two times and fixed with 4% paraformaldehyde for 10 min, and then stained with oil red O solution for 30 min. Finally, the nucleus was stained with hematoxylin and the images were captured with a cell imaging system. PAS staining was carried out with a commercial kit (Cat.: G1281, Solarbio, Beijing, China) according to the manufacturer's protocol, and the images were captured by EVOS FL Auto system (Life TechnologiesTM, Grand Island, NY, USA).

2.7. Transfections of plasmids and small-interfering RNA

Flag-tagged PAQR3 plasmids and HA-tagged DDB2 plasmids were obtained from Vigene Biosciences (Jinan, China). pRK5-HA-Ub (RRID: Addgene_17608), pRK5-HA-Ub-K0 (RRID: Addgene_17603), pRK5-HA-Ub-K48 (RRID: Addgene_17605), and pRK5-HA-Ub-K63 (RRID: Addgene_17606) were obtained from Addgene (Watertown, MA, USA). Plasmids were handled according to the manufacturer's instructions with LTX reagent and

PLUS reagent (ThermoFisher Scientific, Rockford, IL, USA). HepG2 cells were cultured 24 h prior to transfection, and then 2 μg of plasmid was transfected into cells with incubation for 48 h for further treatment.

The siRNA oligonucleotides of *PAQR3* and *DDB2* were purchased from GenePharma (Shuzhou, China), and the most effective sequences are listed in Supporting Information Table S3. Transfection of siRNA was performed according to the manufacturer's instructions with Lipofectamine RNAiMAX reagent (ThermoFisher Scientific). Transfected cells were incubated for 48 h for further treatment.

2.8. Protein extraction and Western blot assay

Liver tissue proteins and HepG2 cells were extracted using RIPA containing 1% (*v*/*v*) protease inhibitor cocktail. The tissues were rapidly separated from the liver on ice and each 0.1 g tissue aliquot was homogenized with 1 mL RIPA buffer, and then lysed for 30 min on ice. The proteins were quantified with a BCA protein assay kit. The proteins (30 μg) were subjected to electrophoresis and detected by Western blotting. Nuclear proteins were extracted by using a nucleoprotein extraction kit and Golgi proteins were extracted with a Golgi extraction kit. Nuclear proteins (10 μg) were loaded for Western blot analysis to detect the nuclear distribution of FOXO1 and SREBP-1c, and 15 μg Golgi proteins were analyzed by Western blotting to detect the distribution of PAQR3 and p110α in Golgi apparatus.

2.9. Quantitative real-time PCR

Total RNA was extracted from HepG2 cells and liver tissues by using trizol (TaKaRa Biotechnology Co., Ltd., Dalian, China) and reversely transcribed into cDNA by reverse transcriptase (ThermoFisher Scientific). Real-time PCR was performed on a Light Cycler 480II real-time PCR detection system (Roche, Shanghai, China) using iTaq Universal SYBR Green Supermix (BioRad, Hercules, CA, USA). The primer sequences are listed in Supporting Information Table S4.

2.10. Measurement of PI3K activity and phosphoinositide (3,4,5)-triphosphate (PIP3) content

HepG2 cells were treated with insulin (100 nmol/L) for the indicated times, and then cells were harvested and lysed with immunoprecipitation lysate buffer (containing with protease inhibitors cocktail, phosphatase inhibitors A and B) on ice for 30 min, followed by centrifugation at 12,000 × *g* for 10 min, 1000 μg of cellular proteins were incubated with 2−5 μg antibodies against IRS-1 overnight at 4 °C with shaking, followed by incubation with 30 μL protein A/G beads for 4 h at 4 °C. The beads were washed with TNE buffer and the PI3K activity was measured in immunoprecipitates with a PI3K ELISA kit (Enzyme-linked Biotechbology Co., Ltd., Shanghai, China). Phosphoinositide (3,4,5)-triphosphate (PIP3) content in the cells was measured with a PIP3 ELISA kit (Enzyme-linked Biotechbology Co., Ltd., Shanghai, China) according to the protocol.

2.11. Immunofluorescence

HepG2 cells were treated with various stimuli, washed with cold PBS for 3 times and fixed with 4% paraformaldehyde for 15 min at room temperature, and then permeabilized with 0.1% TritonX-100 for another 10 min. Cells were blocked with 10% goat serum for 1 h at room temperature, and then incubated with primary antibodies. After washing with PBS, the cells were incubated with Alexa Fluor-conjugated secondary antibody in the dark at room temperature for 1 h. Finally, the nuclei were stained with DAPI solution for 10 min in the dark and the images were captured by using a laser confocal fluorescence microscope (Olympus, Tokyo, Japan).

2.12. Immunoprecipitation assay

HepG2 cells and liver tissues were harvested and lysed with immunoprecipitation lysate buffer (containing with protease inhibitors cocktail, phosphatase inhibitors A and B) on ice for 30 min, and then centrifuged at 12,000 × *g* for 10 min. Cellular proteins (600 μg) and tissue proteins (1000 μg) were incubated with 2−5 μg antibodies overnight at 4 °C with shaking for 8 h, and 20 μL protein agarose A/G beads were added for another incubation for 4 h at 4 °C with shaking. The beads were washed with immunoprecipitation buffer and 20 μL SDS loading buffer was added for Western blotting.

2.13. Molecular docking

The amino acid sequence of PAQR3 (code: Q6TCH7) was obtained from Uniprot. Swiss Model was applied to identify a suitable structure template (PDB, code: 5lxg.1.A), build a homology model and evaluate the model quality. The molecular docking model of GPS with the 3D structure of the PAQR3 homology model was carried out by Molecular Operating Environment 2015 (MOE 2015, Chemical Computing Group ULC). The regularized protein was used in determination of the important amino acids in the predicted binding pocket. Interactive docking for all the conformers of GPS to the selected active site was performed by MOE after energy minimization using prepare ligand protocol. A binding energy was assigned to the docked compound according to its binding mode on the binding site. The protein ligand interaction fingerprint (PLIF) was applied to identify the protein−ligand interaction types.

2.14. His-labeled PAQR3 protein purification

His-labeled PAQR3 plasmids were obtained from Vigene Bioscience. PAQR3-S129T/Y125F/E69D/D42E/L40G and PAQR3-E69Del plasmids were prepared with the QuikChange site-directed mutagenesis kit (Stratagene, La Jolla, CA, USA) by using his-PAQR3 wild-type plasmids as a template. The primers are listed in Table S4. DH5α cells (CD201-01, TransGen Biotech) for cloning and the *Escherichia coli* strain BL 21 (DE3) (CD601-01, TransGen Biotech) were used as the host for prokaryotic expression. Recombinant plasmids encoding His-tagged PAQR3 and PAQR3-Glu^{69}Del were transfected into *E. coli* BL21 (DE3), followed by induction of protein expression by isopropyl β-D-1-thiogalactopyranoside (IPTG, 1.5 mmol/L, 16 °C, 6 h). The proteins were purified with a His-labeled protein purification kit. All preparations were desalted with PD-10 desalting columns (GE Healthcare, 52-1308-00). Proteins were eluted with gradient concentration imidazole (Sangon Biotech, A600277) and enriched by ultrafiltration (MWCO 5 kD, Millipore) and preserved in PBS containing 20% glycerol at −80 °C.

2.15. Surface plasmon resonance (SPR) analysis

SPR measurements were performed on a Biacore 8K instrument (GE Healthcare, Piscataway, NJ, USA). Briefly, purified PAQR3-WT proteins and PAQR3- E69Del proteins (200 mg/mL, pH 4.5) were immobilized (w10000 RU) on a Series S Sensor Chip (GE Healthcare, Piscataway, NJ, USA) according to a standard amine-coupling procedure. PBS (AR1155, pH 7.2−7.4, Boster) with 5% DMSO was used as the running buffer for immobilization. After immobilization, the solution of GPS was prepared with running buffer through serial dilutions of stock solution. Seven concentrations of GPS were injected simultaneously at a flow rate of 65 mL/min for 60 s of association phase at 25 °C. The final graphs were obtained by subtracting blank sensorgrams. Experimental data were collected with the Biacore 8K manager software (GE Healthcare, Piscataway, NJ, USA) and analyzed to fit an appropriate binding model to obtain the equilibrium dissociation constant (K_d).

2.16. Microscale thermophoresis (MST)

As described previously[40], the equilibrium dissociation constant (K_d) values were measured by using the Monolith NT.115 instrument (NanoTemper Technologies). The PAQR3 proteins were fluorescently labeled according to the manufacturer's protocol. GPS was diluted to the indicated concentration (from 5 nmol/L to 1 mmol/L) and incubated with 0.85 mg/mL of purified labeled PAQR3 protein for 15 min in running buffer (50 mmol/L Tris-HCl, 100 mmol/L NaCl, pH 7.5). The samples were loaded into the NanoTemper glass capillaries and microthermophoresis was carried out using 80% light emitting diode power and 80% MST. The K_d values were calculated using the mass action equation *via* the NanoTemper software from duplicate reads of measurements.

2.17. Thermal shift assay (TSA)

As described previously[41], 0.08 mg/mL PAQR3-WT protein was used with or without 0.25 mmol/L GPS in PBS. Data were analyzed with the differential scanning fluorimetry analysis tool (Microsoft Excel-based) by using the curve-fitting software XLfit 5 (www.idbs.com, ID Business Solutions Ltd.).

For the *in vivo* cellular thermal shift assay (CETSA), PAQR3-WT, PAQR3-S129T/Y125F/E69D/D42E/L40G and PAQR3-E69Del plasmids were transiently transfected to HEK 293T cells with LTX reagent and PLUS reagent (Invitrogen). Transfection of HEK 293T cells was performed for 8 h according to the manufacturer's protocol, and the cells were cultured with 80 μmol/L GPS for 2 h. As previously described[40], control cells were incubated with the same volume of PBS. Cells were cultivated and counted, followed by resuspension in PBS (containing 1 mmol/L PMSF) to a final density of 2×10^7/mL. Cells were subpackaged into seven PCR tubes and heated with a thermal gradient from 37 to 67 °C for 3 min. After freeze−thawing twice with liquid nitrogen, the supernatant was separated by centrifugation at 12,000 × *g* for 25 min and collected. A 20 μL aliquot of the supernatant was loaded onto an SDS-PAGE gel, followed by Western blotting. CETSA curve analysis and the thermal stability to reach 50% of temperature (T_{m50}) value were performed using GraphPad Prism software (GraphPad Software Inc., San Diego, CA, USA).

2.18. Serum/hepatic biochemistry measurements and tissue histology

Glycated serum protein (GSP), total cholesterol (T-CHO), triglycerides (TG), LDL cholesterol, HDL cholesterol, alanine aminotransferase (ALT) and aspartate aminotransferase (AST) of serum and hepatic glycogen were measured with kits purchased from Jiancheng Bioengineering Institute (Nanjing, China). Superoxide dismutase (SOD) and malondialdehyde (MDA) were measured with kits purchased from Beyongtime (Haimeng, China). The LW/BW (mg/g) was calculated as the ratio of the weight of the liver and the body weight of the mice.

Liver tissues were fixed with 4% paraformaldehyde and embedded in paraffin, and the embedded sections were prepared to 4 μm thickness. Tissue slices were dehydrated with ethanol in an ascending series and cleared with xylene. Then slices were stained with hematoxylin and eosin (H&E) and periodic acid-Schiff (PAS) for assessing the morphology, degree of inflammation and hepatic glycogen formation. Immunohistochemical staining was applied to observe the expression and cellular distribution of GCK and LDLR in liver. Immunofluorescent staining was utilized to observe the cellular distribution and co-localization of FOXO1, SREBP-1c, PAQR3, DDB2 and p110α in liver tissues. The liver tissues for frozen section were fixed with 4% paraformaldehyde and then prepared into 4 μm-thick slices. The slices were stained with oil red O for assessing the degree of lipid deposition in liver, and the images were captured with a cell imaging system.

2.19. Statistical analysis

The experimental data are all expressed as mean ± standard deviation (SD) and were analyzed by Graphpad Prism 7.0 (GraphPad Software Inc., San Diego, CA, USA). Unpaired Student's *t* test was used to compare between two groups and multiple comparisons were assessed by one-way ANOVA with Turkey' tests. When $P < 0.05$ the difference was considered statistically significant.

3. Results

3.1. GPS decreased lipid synthesis and increased glucose utilization by activating the PI3K/AKT signaling pathway in PA-induced HepG2 cells

Excessive free fatty acids in obese patients contributes to the occurrence and development of insulin resistance[42,43]. Palmitic acid (PA), a saturated fatty acid and main component of free fatty acids, can be used for the induction of insulin resistance in hepatic cells and in skeletal cells[44]. As shown in Fig. S1C, stimulation with 0.25 mmol/L PA for 24 h induced the aberrant expression of GCK, G6pase, LDLR and SREBP-1c in HepG2 cells. Therefore, HepG2 cells with 0.25 mmol/L PA treatment for 24 h were employed in the following experiments. In normal HepG2 cells, GPS showed no obvious toxicity to cells when the concentration was below 320 μmol/L (Fig. S1B).

Flow cytometry results indicated that 80 μmol/LGPS showed similar effects as 250 μmol/L metformin in increasing glucose utilization in PA-treated HepG2 cells (Fig. 1A). In addition, GPS significantly reduced the TG and TC contents in HepG2 cells (Fig. 1B). As illustrated in oil red O staining and PAS staining, GPS treatment reduced lipid droplets deposition and increased glycogen synthesis in PA-treated HepG2 cells (Fig. 1C). Notably,

80 μmol/L GPS showed similar effects on improving glycolipid metabolism with 250 μmol/L metformin. Meanwhile, Western blot results revealed aberrant protein expression of GCK, G6Pase, LDLR and SREBP-1c in HepG2 cells with PA stimulation, while GPS downregulated these glycolipid metabolism markers in a dose-dependent manner (Fig. 1D). Membrane proteins were extracted to detect GLUT4 expression and Western blot results showed that GPS treatment significantly facilitated the membrane translocation of GLUT4 in PA-induced cells, which is important for glucose utilization (Supporting Information Fig. S3A).

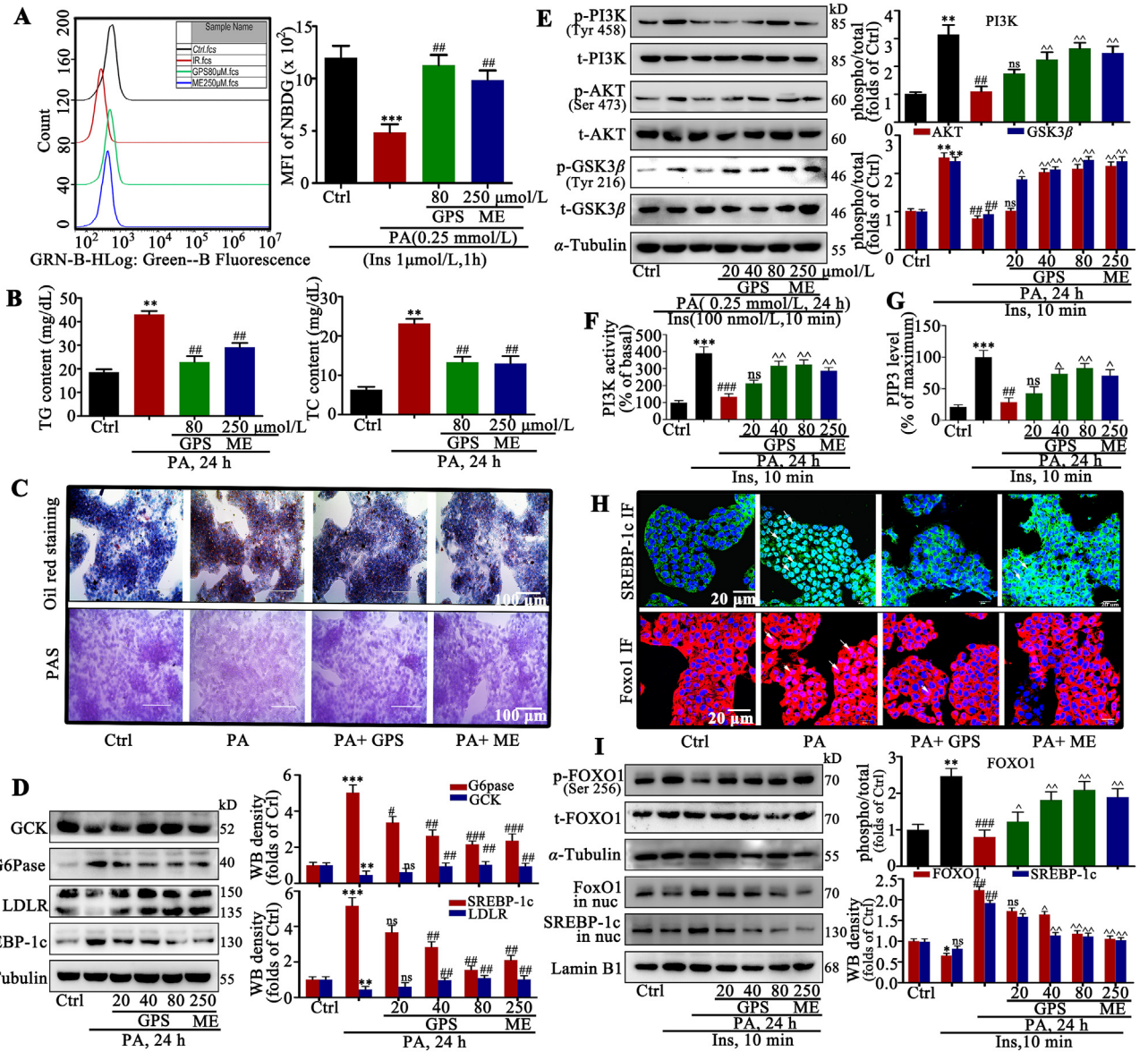

Figure 1 GPS treatment promoted the activation of the PI3K/AKT axis to improve glucose and lipid metabolism in PA-treated HepG2 cells. (A) Glucose uptake assessment in GPS-treated HepG2 cells under palmitate acids conditions ($n = 3$). $^{***}P < 0.001$ *vs.* control group, $^{\#\#}P < 0.01$ *vs.* PA-induced group. (B) TG and TC contents in HepG2 cells ($n = 3$). $^{**}P < 0.01$ *vs.* control group, $^{\#\#}P < 0.01$ *vs.* PA-treated group. (C) Lipid droplets deposition was assessed by oil red staining and glycogen synthesis was assessed by PAS staining. (D) GCK, G6Pase, LDLR and SREBP-1c protein levels in palmitate acid-induced HepG2 cells ($n = 3$). $^{***}P < 0.001$, $^{**}P < 0.01$ *vs.* control group; $^{\#\#\#}P < 0.001$, $^{\#\#}P < 0.01$, $^{\#}P < 0.05$ *vs.* PA-induced group. (E) Effect of GPS on the phosphorylation level of PI3K, AKT and GSK3β ($n = 3$). $^{**}P < 0.01$ *vs.* control group; $^{\#\#}P < 0.01$ *vs.* insulin-induced group; $^{\wedge\wedge}P < 0.01$, $^{\wedge}P < 0.05$ *vs.* PA + insulin-induced group. (F) PI3K activity in GPS co-treated HepG2 cells and (G) PIP3 levels in GPS co-treated HepG2 cells ($n = 3$). $^{***}P < 0.001$ *vs.* control group; $^{\#\#\#}P < 0.001$, $^{\#\#}P < 0.01$ *vs.* insulin-induced group; $^{\wedge\wedge}P < 0.01$, $^{\wedge}P < 0.05$ *vs.* PA + insulin-induced group, ns: no significance. (H) The subcellular distribution of FOXO1 and SREBP-1c was determined by immunofluorescent. Green fluorescence indicates FOXO1, red fluorescence indicates SREBP-1c and blue fluorescence indicates nucleus, scale bar = 20 μm. (I) Phosphorylation of FOXO1 and nuclear distribution of FOXO1 and SREBP-1c were measured by Western blot ($n = 3$). $^{**}P < 0.01$, $^{*}P < 0.05$ *vs.* control group; $^{\#\#\#}P < 0.001$, $^{\#\#}P < 0.01$ *vs.* insulin-induced group; $^{\wedge}P < 0.01$, $^{\wedge}P < 0.05$ *vs.* PA + insulin-induced group. Protein level was quantified and normalized to α-tubulin in the control group cells. The data are presented as mean ± standard deviation (SD), all experiments were performed at least three times with similar results. ns, no significance.

Moreover, 2-NBDG staining revealed that GPS dramatically increased the glucose uptake in PA-induced HepG2 cells (Supporting Information Fig. S3B).

We examined the effects of GPS on PI3K/AKT axis activation, which is important for the regulation of glucose and lipid metabolism. Results of ELISA showed that stimulation with 100 nmol/L insulin rapidly facilitated PIP3 production with the maximum amount at 10 min in HepG2 cells (Fig. S1D), thus stimulation with 100 nmol/L insulin for 10 min was used in the subsequent experiments to activate the insulin signaling pathway. Results of Western blotting showed that impaired PI3K (the phosphorylated forms at Tyr458), AKT (the phosphorylated forms at Ser473) and GSK3β (the phosphorylated Tyr216) signaling induced by PA stimulation was restored by GPS co-treatment, when it was stimulated by insulin (Fig. 1E). In addition, as shown in Fig. 1F and G, PA stimulation remarkably inhibited PI3K activity and reduced PIP3 production in insulin-treated HepG2 cells, while GPS co-treatment could restore PI3K activity and promoted PIP3 production. FOXO1 and SREBP-1c are the main transcription factors that regulate the transcription of proteins such as GCK, G6Pase, PEPCK and LDLR in the insulin signaling pathway[12,13]. Under the condition of insulin resistance, phosphorylated FOXO1 and SREBP-1c were aggregated in the nucleus, reducing the synthesis of GCK and LDLR and promoting the synthesis of G6Pase, which contributes to glycogen decomposition and lipid synthesis. As shown in Fig. 1H, immunofluorescence images revealed a pronounced enrichment of FOXO1 and SREBP-1c in the nucleus of PA-treated cells compared with control cells, while GPS co-treatment effectively blocked FOXO1 and SREBP-1c nuclear translocation in PA-treated HepG2 cells. Furthermore, Western blot results showed that GPS reduced the phosphorylated form of FOXO1 and inhibited the nuclear distribution of FOXO1 and SREBP-1c in PA-induced HepG2 cells (Fig. 1I), which were consistent with the immunofluorescence results.

3.2. *GPS promoted the activation of the PI3K/AKT signaling pathway by inhibiting the interaction between PAQR3 and P110α pathway in vitro*

To further examine the role of GPS on the PI3K/AKT axis, we used a specific inhibitor of PI3K (LY294002) in PA-treated HepG2 cells. As illustrated in Fig. 2A, the pre-incubation with LY294002 remarkably reversed the increased phosphorylation of PI3K, AKT and GSK3β induced by GPS co-treatment in PA-treated HepG2 cells, indicating that GPS functionally interacted with PI3K to induce the insulin pathway. Surprisingly, neither PA stimulation nor GPS treatment influenced the mRNA levels of *INSR* and *IRS1* in HepG2 cells (Supporting Information Fig. S4A and S4B). In addition, PA stimulation impaired the expression of INSR and the phosphorylation of IRS-1, which could not be restored by GPS treatment (Fig. S4C).

It is of interest how GPS exactly regulates the activity of PI3K. Recent studies have shown that PAQR3 competitively tethered the catalytic subunit (p110α) of PI3K in the Golgi apparatus to inhibit the formation of the p110α−p85α dimer, which negatively regulated the insulin signaling pathway[28]. Our results show that the *PAQR3* mRNA level was increased significantly in PA-treated HepG2 cells and in liver tissue of diabetic mice (Fig. S4D and S4E). In addition, PAQR3 protein expression was up-regulated in Golgi apparatus in HepG2 cells with PA stimulation in a time-dependent way (Fig. 2B). Additionally, the Western blot results showed that GPS treatment significantly reduced the distribution of PAQR3 and p110α in the Golgi apparatus in PA-treated cells (Fig. 2C). Moreover, co-IP results verified that the interaction of PAQR3 and p110α was significantly increased by PA stimulation in HepG2 cells, while treatment with 80 μmol/L GPS reduced the interaction between PAQR3 and p110α (Fig. 2D). Furthermore, as illustrated in Fig. 2E, cellular immunofluorescence images revealed a pronounced co-localization of PAQR3 and p110α in the Golgi apparatus compared to the control group, while GPS treatment remarkably reduced the co-localization of PAQR3 and p110α in the Golgi apparatus. Meanwhile, co-IP results indicated that GPS treatment significantly increased the interaction between p110α and p85α in PA-treated HepG2 cells, implying that GPS treatment promoted the formation of a PI3K dimer (Fig. 2F).

Overexpression with *PAQR3* plasmids and knockdown with *PAQR3* siRNA were applied to examine the role of PAQR3 in GPS-induced PI3K activation. Results show that *PAQR3* overexpression remarkably reversed the effects of GPS treatment on reducing the distribution of PAQR3 and P110α in the Golgi apparatus (Fig. 2G). In addition, PAQR3 overexpression nearly abolished the formation of the PI3K dimer (P110α−P85α) induced by GPS co-treatment (Fig. 2H). As expected, the activation of PI3K/AKT axis induced by GPS was also reversed by *PAQR3* overexpression (Fig. 2I and Supporting Information Fig. S5A). Meanwhile, *PAQR3* overexpression impaired the regulation of GPS in glycolipid metabolism (Fig. S5B). Moreover, the results demonstrate that *PAQR3* knockdown was sufficient to restore the PI3K/AKT axis and improve glycolipid metabolism marker expression, whereas co-treatment with GPS did not produce an additional effect (Supporting Information Fig. S6A−S6E).

3.3. *GPS inhibited PAQR3 protein expression via DDB2-mediated ubiquitination of PAQR3 in vitro*

We investigated the mechanism through which GPS negatively regulates the PAQR3 protein level. Real-time PCR analysis indicated that GPS did not regulate the mRNA level of *PAQR3* in PA-treated HepG2 cells (Fig. 3A), implying that GPS down-regulated PAQR3 expression was not transcription-dependent. In addition, these results were further confirmed by half-life analysis of PAQR3. HepG2 cells were exposed to the protein translation inhibitor (CHX) with/without GPS. The half-life analysis showed that the turnover rate of PAQR3 in the GPS-treated group was faster than in the untreated group, suggesting that GPS regulated PAQR3 expression at the post-translational level (Fig. 3B).

It has been reported that PAQR3 could be degraded by the ubiquitin−proteasome pathway[32], but the ubiquitination degradation mechanisms of PAQR3 remains unclear. Therefore, we further explored the mechanisms of PAQR3 degradation. We found that treatment with MG132, a proteasome inhibitor, could block the degradation of PAQR3 protein in HepG2 cells in the presence of the protein synthesis inhibitor cycloheximide (CHX), while the lysosome inhibitor chloroquine (CQ) failed to prevent PAQR3 degradation (Supporting Information Fig. S7A). This result clarified that PAQR3 degradation is mediated by proteasome. Moreover, we found that PAQR3 could be polyubiquitinated

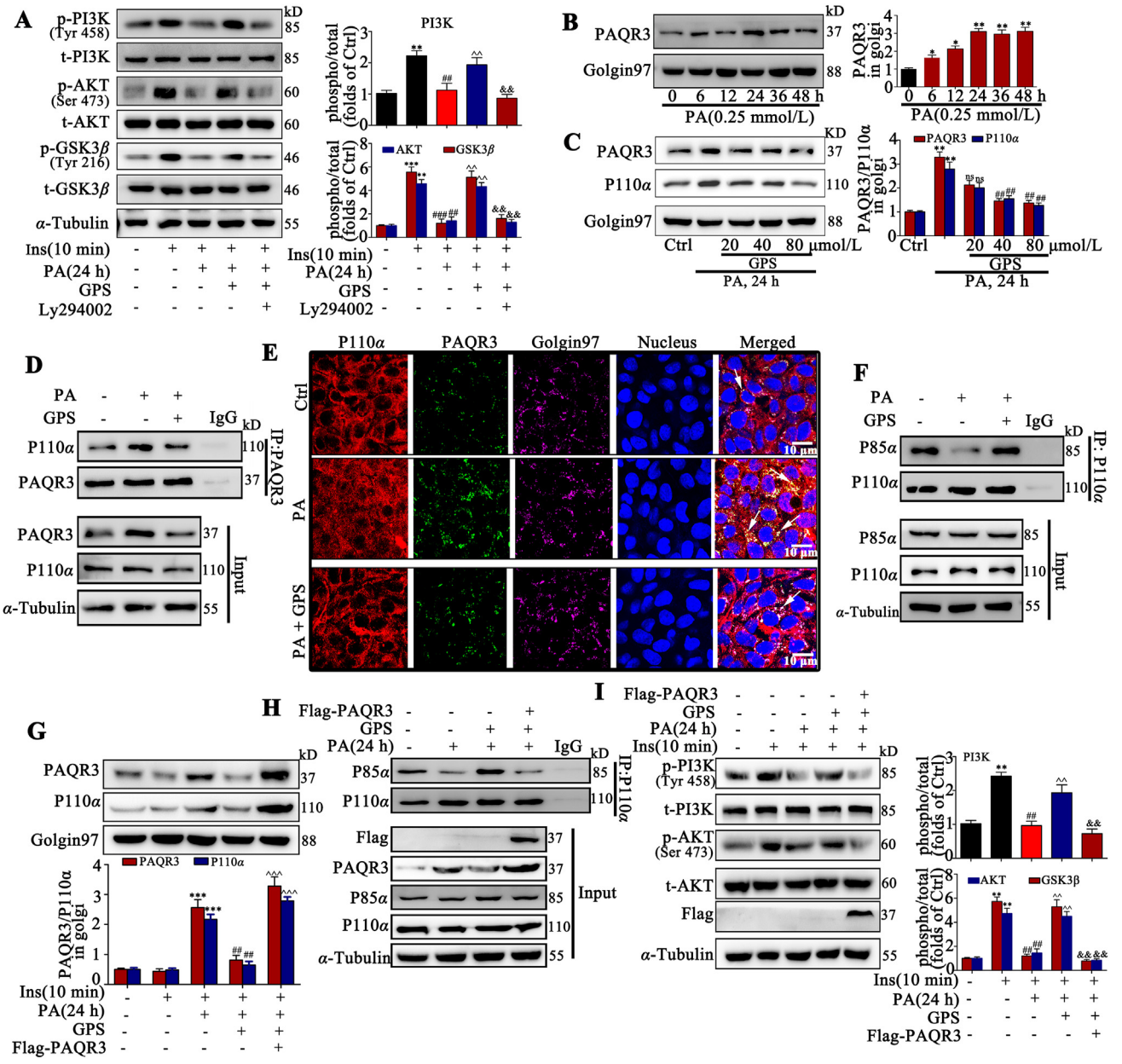

Figure 2 GPS inhibited the interaction between PAQR3 and P110α to promote the activation of the PI3K/AKT pathway *in vitro*. (A) LY294002 reversed the up-regulation of p-PI3K, p-AKT and p-GSK3β induced by GPS co-treatment in PA-treated HepG2 cells ($n = 3$). $^{***}P < 0.001$, $^{**}P < 0.01$ *vs.* control group; $^{\#\#\#}P < 0.001$, $^{\#\#}P < 0.01$ *vs.* insulin-induced group; $^{\wedge}P < 0.01$ *vs.* PA + insulin-induced group; $^{\&\&}P < 0.01$ *vs.* insulin + PA + GPS-treated group. (B) Palmitatic acid stimulation increased the protein expression of PAQR3 in the Golgi apparatus in a time-dependent manner ($n = 3$). $^{**}P < 0.01$, $^{*}P < 0.05$ *vs.* 0 h. (C) The expression of PAQR3 and p110α in the Golgi apparatus in GPS co-treated HepG2 cells ($n = 3$). $^{**}P < 0.01$ *vs.* Control group; $^{\#\#}P < 0.01$ *vs.* PA-induced group, ns: no significance. (D) A co-immunoprecipitation assay was performed to detect the combination of PAQR3 and p110α *in vitro*. (E) Immunofluorescence staining presented the distribution and co-localization of PAQR3 and P110α in HepG2 cells, scale bar = 20 μm. (F) A co-immunoprecipitation assay was performed to detect the combination of p110α and p85α in HepG2 cells. (G) The expression of PAQR3 and p110α in the Golgi apparatus of HepG2 cells ($n = 3$). $^{***}P < 0.001$ *vs.* control group; $^{\#\#}P < 0.01$ *vs.* PA-induced group; $^{\wedge}P < 0.001$ *vs.* PA + GPS-treated group. (H) The interaction between P110α and P85α in PA-treated HepG2 cells. (I) PAQR3 overexpression reversed the up-regulation of p-PI3K and p-AKT in PA-induced HepG2 cells ($n = 3$). $^{**}P < 0.01$ *vs.* control group; $^{\#\#}P < 0.01$ *vs.* insulin-induced group; $^{\wedge}P < 0.01$ *vs.* PA + insulin-induced group; $^{\&\&}P < 0.01$ *vs.* PA + insulin + GPS treated group. Protein level was quantified and normalized to α-tubulin in the control group cells. The data are presented as mean ± SD, and all experiments were performed at least three times with similar results. ns, no significance.

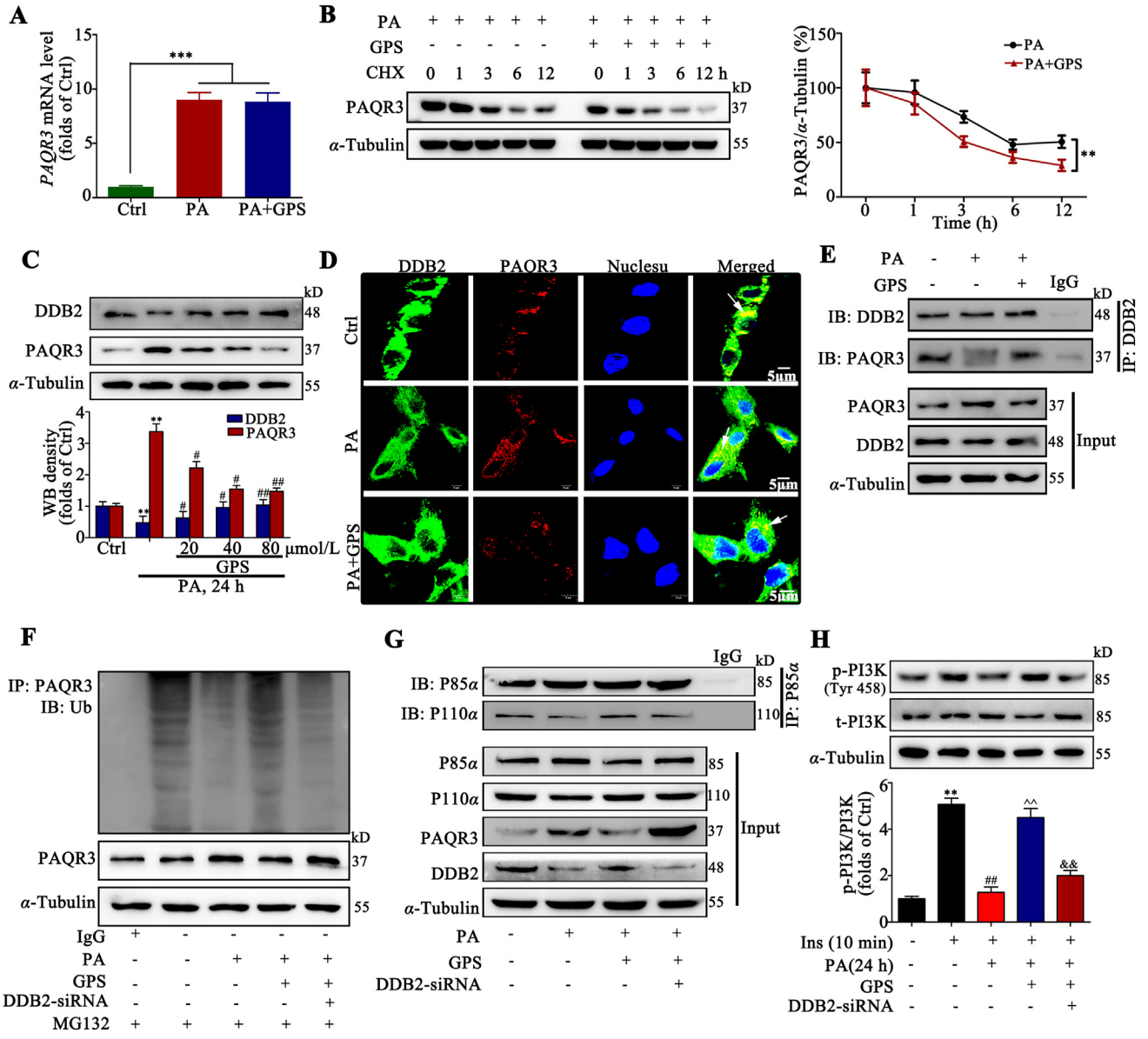

Figure 3 GPS increased the ubiquitination of PAQR3 by promoting the interaction between DDB2 and PAQR3. (A) *PAQR3* mRNA level in HepG2 cells ($n = 3$). $^{***}P < 0.001$ *vs.* Ctrl. (B) The protein level of PAQR3 was determined by Western blot assay with HepG2 cells treated with PA and/or GPS in the presence of CHX (50 mg/mL) for 0, 1, 2, 4, 6, and 12 h ($n = 3$). $^{**}P < 0.001$ *vs.* PA-treated group. (C) DDB2 and PAQR3 protein expression in HepG2 cells ($n = 3$). $^{**}P < 0.01$ *vs.* Ctrl; $^{\#}P < 0.05$, $^{\#\#}P < 0.01$ *vs.* PA-treated group. (D) Immunofluorescence staining presents the distribution and co-location of DDB2 and PAQR3 in HepG2 cells, scale bar = 20 μm. (E) A co-immunoprecipitation assay was performed to detect the interaction of DDB2 and PAQR3 in HepG2 cells. (F) Knockdown *DDB2* decreased the polyubiquitination of PAQR3 induced by GPS in HepG2 cells. (G) The interaction of p85α and p110α when HepG2 cells were treated with PA and/or GPS, in the presence of *PAQR3* siRNA. (H) Phosphorylation level of PI3K in HepG2 cells ($n = 3$). $^{**}P < 0.01$ *vs.* Ctrl; $^{\#\#}P < 0.01$ *vs.* insulin-treated group; $^{\wedge}P < 0.01$ *vs.* insulin + PA-treated group; $^{\&\&}P < 0.01$ *vs.* insulin + PA + GPS-treated group. Protein was quantified and normalized to α-tubulin in the control group cells. The data are presented as mean ± SD, all experiments were performed at least three times with similar results.

(Fig. S7B), and the result is consistent with previous reports[32]. Our results show that the ubiquitination of PAQR3 after the co-transfection of HA-Ub-K48 was comparable to that of HA-Ub, while the co-transfection of HA-Ub-K63 failed to increase the ubiquitination of PAQR3 in HEK 293A cells exposed to MG132 (Fig. S7C), suggesting that PAQR3 is modified mainly by K48-linked polyubiquitination.

To clarify the mechanism of enhanced PAQR3-specific ubiquitination induced by GPS co-treatment, we focused on the role of DDB2, a substrate receptor module that determines the specificity of targeted substrate for ubiquitination[45]. Recent studies have suggested that DDB2 is a post-transcriptional regulator of PAQR3, which promotes the ubiquitin-mediated degradation of PAQR3[32]. Here, our results show that PAQR3 ubiquitination was inhibited in the presence of PA, while DDB2 overexpression triggered PAQR3 ubiquitination in PA-treated HepG2 cells (Fig. S7D). In addition, our results show that the impaired PI3K (the forms phosphorylated at Tyr458) was largely restored by DDB2 overexpression in PA-

treated cells (Fig. S7E). These results indicate the role of DDB2 in promoting PAQR3 ubiquitination to restore PI3K activation.

However, whether GPS promoted PAQR3 ubiquitination degradation *via* regulating DDB2 remains unclear. Our results show that DDB2 was down-regulated and PAQR3 was up-regulated by PA stimulation, while GPS co-treatment significantly increased DDB2 expression and decreased PAQR3 expression (Fig. 3C). Real-time PCR assay indicated that GPS significantly increased the mRNA level of *DDB2* in PA-treated HepG2 cells, implying the up-regulation of DDB2 expression induced by GPS is a transcriptional event (Fig. S7F). In addition, cellular immunofluorescence images revealed a decreased co-localization of DDB2 and PAQR3 in PA-treated cells compared to the control group, while GPS co-treatment remarkably increased the co-localization of DDB2 and PAQR3 in PA-treated cells (Fig. 3D). Co-IP results verified that GPS could promote the interaction between DDB2 and PAQR3 in PA-treated cells (Fig. 3E). Notably, GPS-induced ubiquitination of PAQR3 was largely impaired by *DDB2*-siRNA (Fig. 3F). Meanwhile, *DDB2* knockdown largely impaired the effects of GPS on promoting the interaction between P110α and P85α in PA-treated HepG2 cells (Fig. 3G). Furthermore, *DDB2* knockdown remarkably impaired the phosphorylation of PI3K induced by GPS co-treatment in insulin−PA-treated cells (Fig. 3H). Taken together, these results suggest that GPS inhibited PAQR3 expression *via* DDB2-mediated PAQR3 ubiquitin degradation.

3.4. *GPS directly targeted the NH_2-terminus of PAQR3*

Co-IP results showed that the overexpression of *DDB2* could reduce the expression of PAQR3 and inhibit the interaction between PAQR3 and P110α, while co-treatment with GPS did not further inhibit the expression of PAQR3, but exerted additional effects to inhibit the interaction between PAQR3 and P110α (Supporting Information Fig. S8A). These results suggest that GPS could further inhibit the interaction between PAQR3 and P110α independently of the inhibition of PAQR3 expression, and whether this effect could be attributed to the direct binding of GPS and PAQR3 remained unclear.

To further investigate the direct interaction between GPS and PAQR3 protein, we performed biophysical assays, SPR, MST and TSA by using recombinant PAQR3 protein from a eukaryotic expression system (Supporting Information Fig. S9A−S9D). SPR results show that GPS directly interacted with PAQR3 protein in a positive dose-dependent manner. The determined equilibrium dissociation constant (K_d) for GPS binding to the PAQR3 protein was 36.7 μmol/L (Fig. 4A). MST, a method that allows the determination of K_d values in solution and requires PAQR3 to be fluorescently labeled, was performed with increasing concentrations of GPS (dilutions from 5 nmol/L to 1 mmol/L) with a constant amount of PAQR3 protein. The results show that increasing amounts of GPS clearly affect the thermophoretic motion of PAQR3; GPS binding to PAQR3 protein yielded K_d values of 43.5 ± 0.26 μmol/L (Fig. 4B). Results from TSA found that upon binding with GPS, the melting temperature of PAQR3 was elevated from ∼55 to ∼60 °C (Fig. 4C).

Next, we investigated the binding site of GPS on PAQR3. Molecular docking of GPS into the binding site of PAQR3 was performed with a homology model of PAQR3 (Supporting Information Fig. S10A−S10C). The docking simulation showed that the binding energy between GPS and PAQR3 is −18.6 kmol/L 3D images reveal that GPS bound to the binding pocket, which formed with amino acids of the PAQR3 NH_2-terminus (Fig. 4D). Magnified 2D images reveal that GPS complex formed seven key hydrogen bonds with Leu40, Asp42, Glu69, Tyr125 and Ser129 of PAQR3 to stabilize the binding conformation, which is important for the inhibitory activity of GPS (Fig. 4E). Notably, a protein ligand interaction fingerprint (PLIF) calculation showed that there are two strong hydrogen bond interactions and strong surface contacts between GPS and Glu69, implying that Glu69 probably serves as an important binding site for GPS (Fig. S10D−S10F).

Using site-directed mutagenesis, we constructed PAQR3-S129T/Y125F/E69D/D42E/L40G and PAQR3-E69Del mutant of PAQR3. CETSA with HEK293T cells demonstrated that GPS largely improved the thermal stability of exogenous wild-type PAQR3 (PAQR3-WT), while GPS did not change the thermal stability of exogenous PAQR3-S129T/Y125F/E69D/D42E/L40G, indicating Leu40, Asp42, Glu69, Tyr125 and Ser129 might be responsible for the interaction between PAQR3 and GPS (Fig. 4F and G), as predicted by molecular docking. Furthermore, the increased thermal stability of PAQR3 induced by GPS was largely impaired by the deletion of Glu69 (Fig. 4F and G). In addition, SPR results showed that the capacity of Glu69-deleted PAQR3 proteins to interact with GPS was remarkably impaired compared to PAQR3-WT proteins, and the K_d value could not be calculated, demonstrating that Glu69 probably serves an important binding site for GPS (Supporting Information Fig. S11A). It has been reported that the NH_2-terminal 71 amino acids of PAQR3 are sufficient to mediate the interaction with p110α and the NH_2-terminus of PAQR3 is sufficient to mediate the inhibitory effect of PAQR3 on insulin signaling[28]. These results indicate GPS can directly bind to PAQR3, and the N-terminus of PAQR3 is an important binding site for GPS.

3.5. *GPS improved glycolipid metabolism disorder by activating the PI3K/AKT signaling pathway in diabetic mice*

Streptozotocin (STZ) and high fat diet (HFD)-induced diabetic mice were used to confirm the effects of GPS *in vivo*. We observed that GPS reduced the fasting blood glucose (FBG) level stably during administration and decreased glycated serum protein (GSP) significantly compared with the diabetes group (Fig. 5A). Additionally, the results show that GPS significantly reduced the ratio of liver weight/body weight (LW/BW), increased the content of hepatic glycogen and reduced total cholesterol (TC) and triglyceride (TG) content in liver tissue (Fig. 5B and C). Moreover, triglyceride (TG), low density lipoprotein cholesterol (LDL-C) and high-density lipoprotein cholesterol (HDL-C) in serum were also improved by GPS treatment for 8 weeks, while neither GPS nor metformin showed an improvement in total cholesterol (TC) (Supporting Information Fig. S12A−S12D). Notably, the oxidative stress caused by antioxidant imbalance will further aggravate insulin resistance[46]. The results show that the content of superoxide dismutase (SOD) is decreased and the production of malondialdehyde (MDA) caused by lipid peroxidation is significantly increased in diabetic mice, while GPS increased the content of SOD and reduced the level of MDA in the serum of diabetic mice (Fig. 5D). Additionally, GPS significantly inhibited the activity of alanine aminotransferase (ALT) and aspartate aminotransferase (AST) compared with the diabetic group (Fig. S12E and S12F). Importantly, our results show that 100 mg/kg GPS is comparable to 195 mg/kg metformin, a first-line agent for the treatment of type II diabetes, in improving glucose and lipid metabolism.

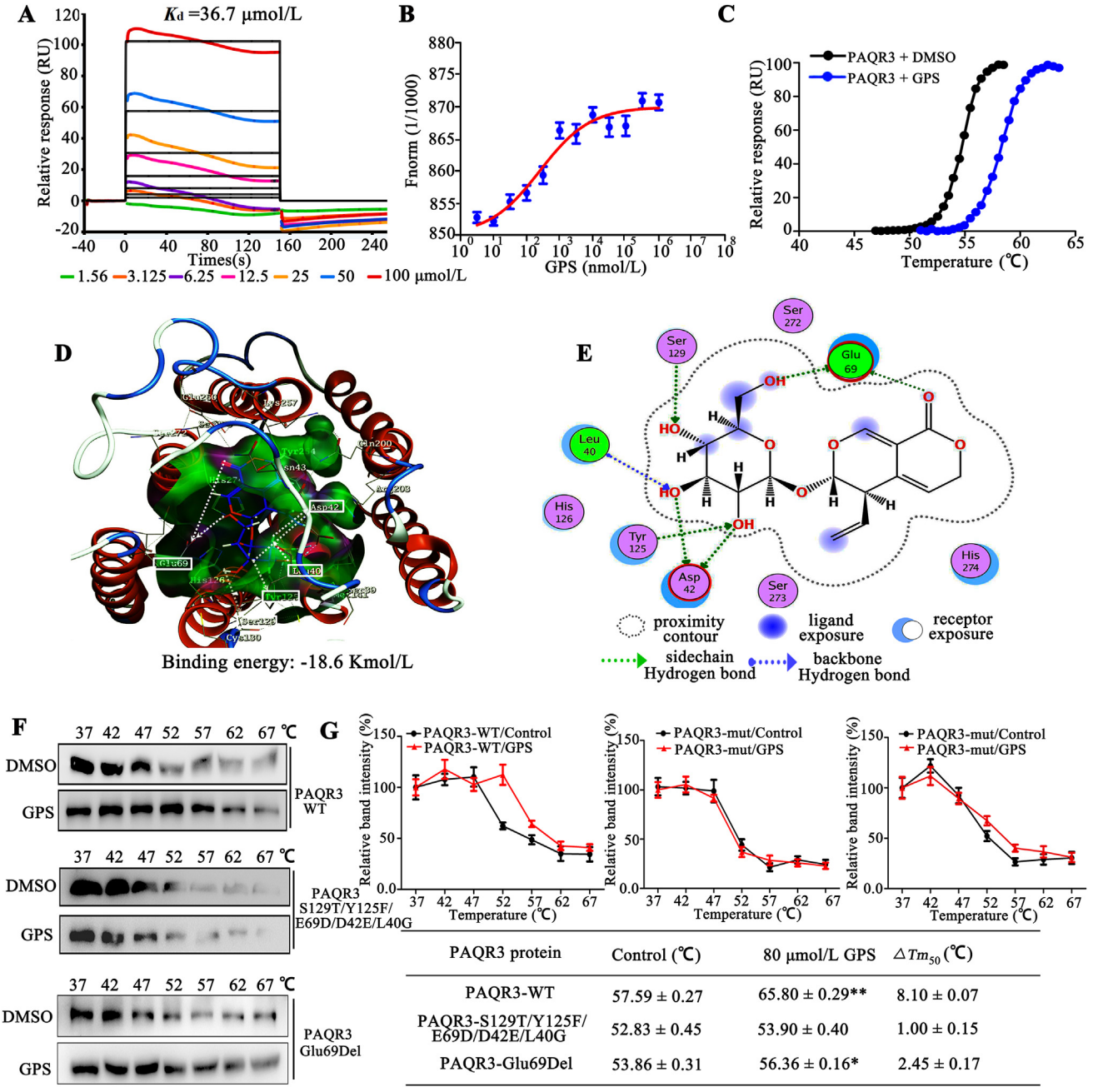

PAQR3 protein	Control (℃)	80 μmol/L GPS	ΔTm_{50} (℃)
PAQR3-WT	57.59 ± 0.27	65.80 ± 0.29**	8.10 ± 0.07
PAQR3-S129T/Y125F/ E69D/D42E/L40G	52.83 ± 0.45	53.90 ± 0.40	1.00 ± 0.15
PAQR3-Glu69Del	53.86 ± 0.31	56.36 ± 0.16*	2.45 ± 0.17

Figure 4 PAQR3 binds GPS. (A) SPR analysis of the binding affinity of GPS to PAQR3 protein. Apparent equilibrium dissociation constants (K_d) were calculated as the ratio of k_d/k_a. The K_d (mol/L) value between GPS and PAQR3 was 3.67×10^{-5} mol/L. (B) Microscale thermophoresis (MST) of GPS. PAQR3 (0.85 mg/mL) was incubated with increasing concentrations of GPS. (C) TSA results in the presence or absence of GPS. (D) The 3D image revealed that GPS bond to the binding pocket, which formed with N-terminal residues of PAQR3. (E) The 2D image reveals that GPS interacts with several amino acids including Leu40, Asp42, Glu69, Tyr125 and Ser129. Green and blue dotted line signifies a hydrogen bond. (F) Cellular thermal shift assay (CETSA) presented the thermal stability of wild-type PAQR3 (PAQR3-WT), and PAQR3-S129T/Y125F/ E69D/D42E/L40G and PAQR3-E69Del plasmid mutant proteins after treatment with GPS (80 μmol/L). (G) CETSA curve and the thermal stability to reach 50% of temperature (T_{m50}) value was performed using GraphPad Prism software. Data are expressed as mean ± SD; $^*P < 0.05$, $^{**}P < 0.01$ *vs.* control group.

We further observed the morphology of liver in diabetic mice. Hematoxylin and eosin (H&E) staining and oil red O staining both showed pathological liver injury and lipid deposition in the liver tissue of diabetic mice, which was improved significantly by GPS or metformin treatment for 8 weeks (Fig. 5E). Additionally, periodic acid-Schiff (PAS) staining showed that GPS treatment effectively increased the content of hepatic glycogen (Fig. S12G). Moreover, as illustrated in the immunohistochemical images, GPS treatment increased the distribution of LDLR and GCK in liver (Fig. 5F). Western blot assay further verified that impaired AKT (the phosphorylated forms at Ser473) and GSK3β (the phosphorylated form at Tyr216) signaling induced by STZ-HFD was restored by GPS administration (Fig. 5G). As expected, GPS treatment improved the expression of glycolipid metabolism

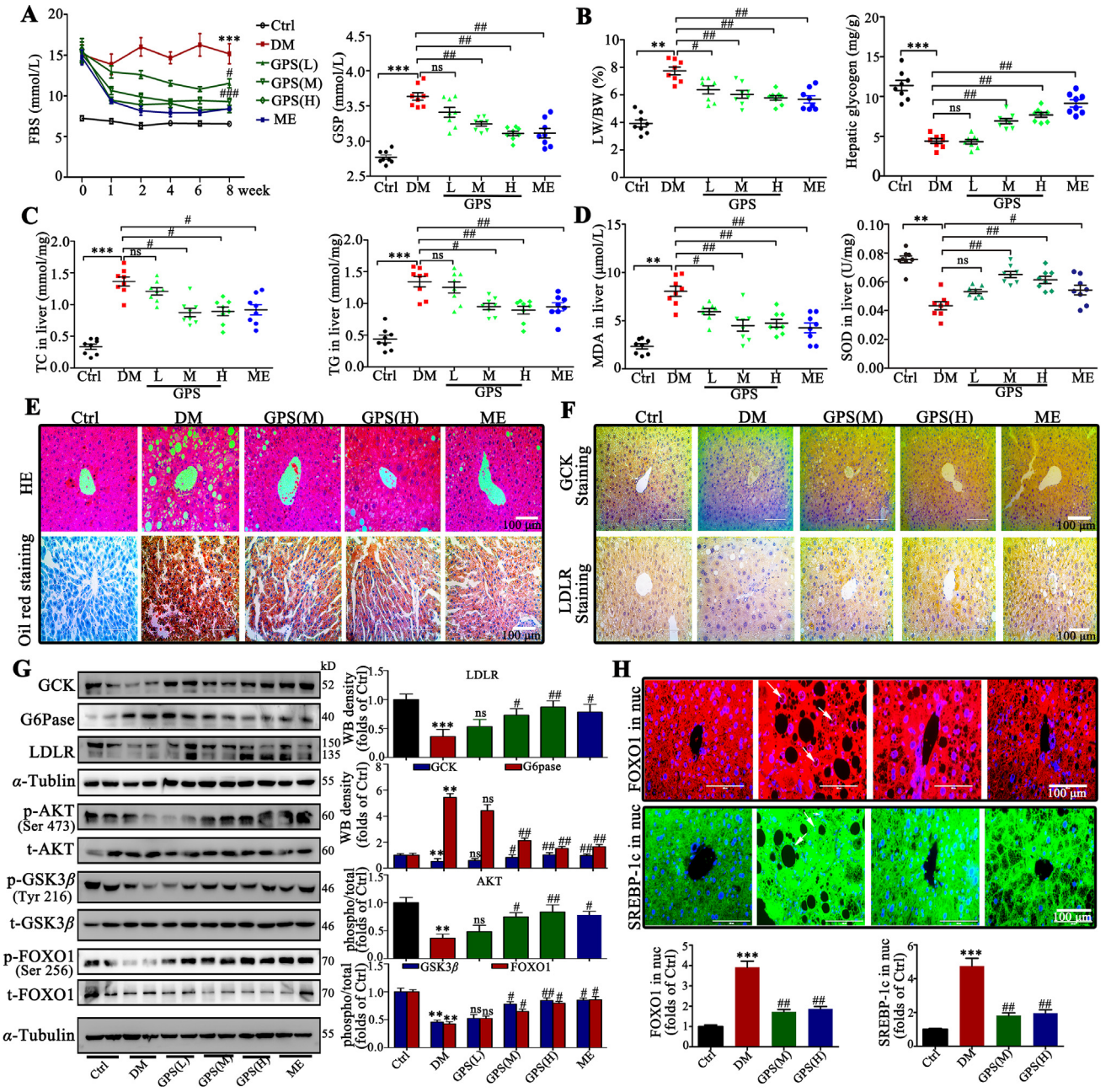

Figure 5 GPS improved glucose and lipid metabolism by activating the PI3K/AKT signaling pathway in diabetic mice. (A) GPS improved blood glucose and GSP in mice treated with STZ and HFD from Week 1 to Week 8 ($n = 8$). (B) Changes in LW/BW and hepatic glycogen content in diabetic mice, LW/BW: liver weight/body weight ratio ($n = 8$). (C) Changes in TC and total TG in liver tissue of diabetic mice ($n = 8$). (D) Changes in MDA content and total SOD activity in liver tissue of diabetic mice ($n = 8$). (E) Representative H&E and oil red O staining images in liver. Scale bar = 100 μm. (F) Representative immunohistochemical staining images of GCK and LDLR in liver. Scale bar = 100 μm. (G) Representative Western blots results and densitometric analysis of mouse glycolipid metabolism markers including GCK, G6Pase, LDLR and SREBP-1c ($n = 8$). (H) The subcellular distribution of FOXO1 and SREBP-1c was determined by immunofluorescent staining; immunofluorescent intensity was analyzed by Image-pro-plus 6.0. Green fluorescence indicates FOXO1, red fluorescence indicates SREBP-1c and blue fluorescence indicates nucleus. Scale bar = 100 μm. Data are expressed as mean ± SD ($n = 8$). Diabetes: diabetes group; GPS (L): 25 mg/kg gentiopicroside; GPS (M): 50 mg/kg gentiopicroside. GPS (H): 100 mg/kg gentiopicroside; ME: 195 mg/kg metformin. $^{***}P < 0.001$, $^{**}P < 0.01$ *vs.* control group; $^{\#\#\#}P < 0.001$, $^{\#\#}P < 0.01$, $^{\#}P < 0.05$ *vs.* diabetes group; ns means no significance.

marker (GCK, G6Pase, LDLR and SREBP-1c) in liver (Fig. 5G). In addition, immunofluorescence images revealed that GPS administration effectively blocked the accumulation of FOXO1 and SREBP-1c in the nucleus of hepatocyte (Fig. 5H). Notably, GPS also inhibited the production of inflammatory adhesion molecules (ICAM-1 and VCAM-1) (Fig. S12H) and intercellular matrix (fibronectin and collagen IV) in liver (Fig. S12I), revealing a protective role for GPS in fatty liver fibrosis.

3.6. *GPS promoted the activation of PI3K by inhibiting PAQR3 expression in vivo*

The *in vitro* results indicated that the inhibition of PAQR3 induced by GPS mediated its protective role in insulin resistance. We further clarified the findings observed in diabetic mice, as illustrated in Fig. 6A. PAQR3 expression was up-regulated and PI3K phosphorylation was down-regulated in liver tissues of diabetic mice compared with the control group, which was reversed by GPS treatment for 8 weeks. Additionally, the Golgi apparatus of liver tissue was extracted and the Western blot results show that GPS reduced the expression of PAQR3 and p110α in the Golgi apparatus (Fig. 6B). An immunofluorescence assay further verified that the co-localization of p110α and PAQR3 was significantly increased in liver under diabetic conditions, while GPS treatment for 8 weeks effectively reduced the co-location of PAQR3 and p110α (Fig. 6C). Co-IP results further verified that the increased interaction between PAQR3 and p110α was inhibited strongly (Fig. 6D) and the interaction between P110α and P85α was increased (Fig. 6E) by GPS treatment in diabetic mice, which was consistent with the *in vitro* results.

3.7. *GPS promoted PAQR3 ubiquitinated degradation by facilitating the interaction between DDB2 and PAQR3 in vivo*

Consistent with the cell experiments, GPS showed no effects on the mRNA level of *Paqr3* in diabetic mice (Fig. 7A), verifying that GPS-inhibited PAQR3 expression was not a transcriptional

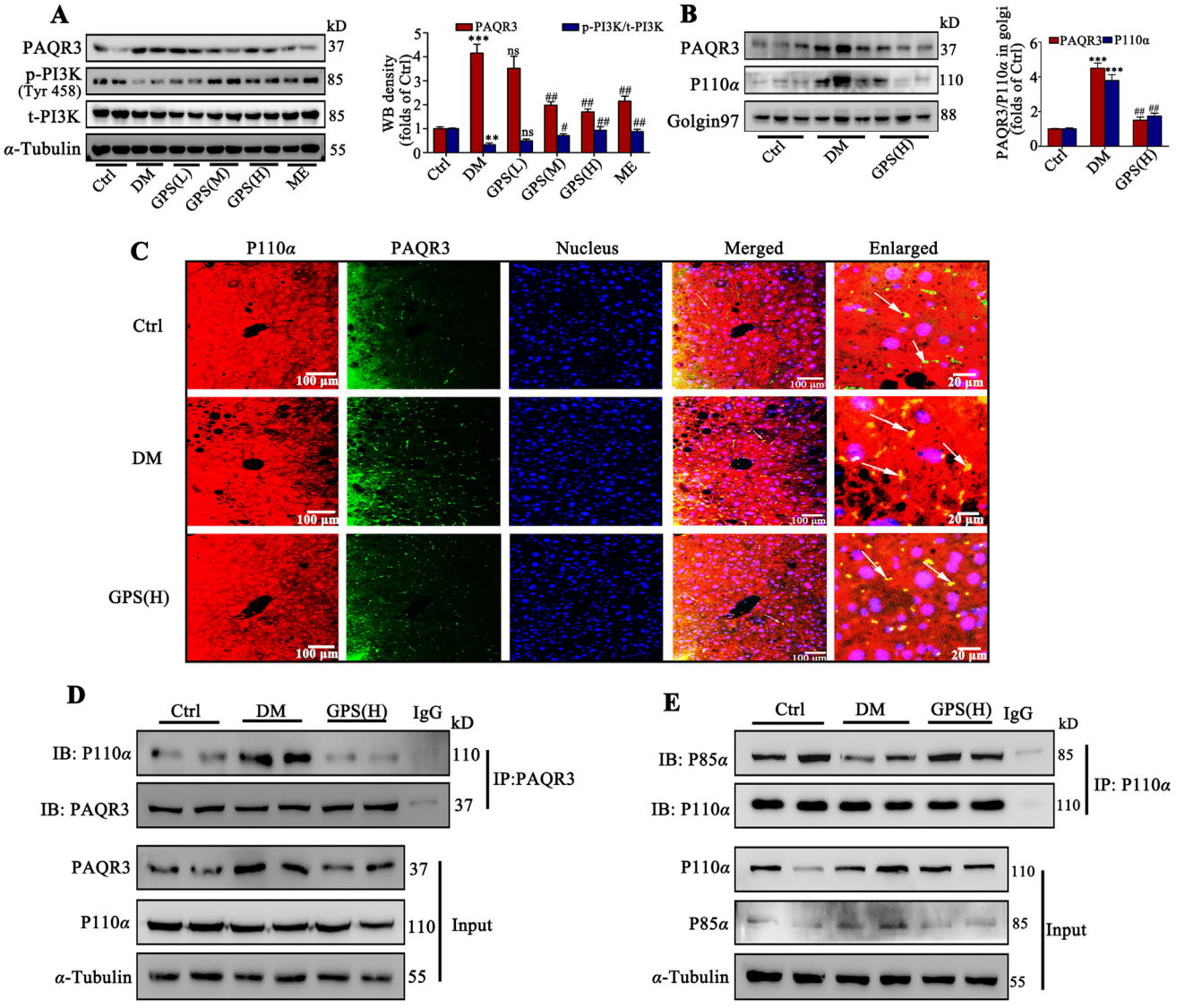

Figure 6 GPS promoted the formation of the PI3K dimer complex (p110α−p85α) in liver tissue by inhibition of PAQR3. (A) Representative Western blots results and densitometric analysis of PAQR3 and p-PI3K in liver tissues ($n = 3$). (B) Representative Western blot results and densitometric analysis of PAQR3 and P110α in Golgi apparatus of liver tissue ($n = 3$). (C) Immunofluorescence staining presents the distribution and co-location of PAQR3 and P110α in liver tissue. Scale bar = 20 μm. (D) A co-immunoprecipitation assay was performed to detect the interaction between PAQR3 and p110α in liver tissue. (E) The interaction between P110α and P85α in liver tissue was detected by co-immunoprecipitation. The data are presented as mean ± SD, all experiments were performed at least three times with similar results. $^{***}P < 0.001$, $^{**}P < 0.01$ *vs.* control group; $^{\#\#}P < 0.01$, $^{\#}P < 0.05$ *vs.* diabetes group; ns means no significance.

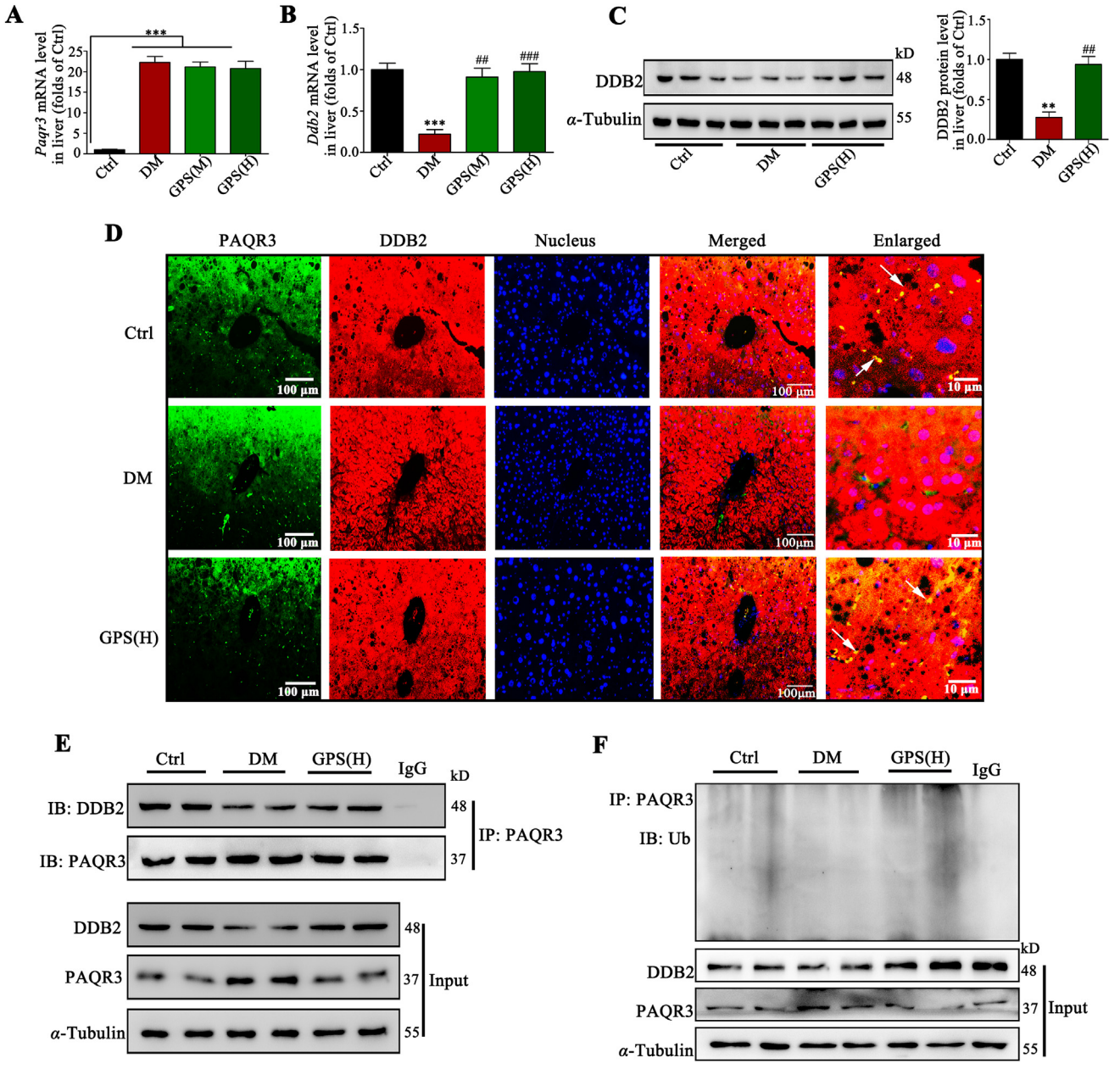

Figure 7 GPS promoted the interaction between DDB2 and PAQR3 to increase PAQR3 ubiquitin-mediated degradation *in vivo*. (A) and (B) *Paqr3* and *Ddb2* mRNA level in liver tissue ($n = 3$). (C) Representative Western blots and densitometric analysis of DDB2 protein level in liver tissue ($n = 3$). (D) Immunofluorescence staining presents the distribution and co-localization of PAQR3 and DDB2 in liver tissue. Scale bar = 100 μm. (E) A co-immunoprecipitation assay was performed to detect the interaction between DDB2 and PAQR3 in liver tissue. (F) GPS promoted the polyubiquitination of PAQR3 in liver tissue. Data are presented as mean ± SD, all experiments were performed at least three times with similar results. $^{***}P < 0.001$, $^{**}P < 0.01$ *vs.* control group; $^{\#\#\#}P < 0.001$, $^{\#\#}P < 0.01$ *vs.* diabetes group; ns: no significance.

event. In addition, real-time PCR assay indicated that GPS significantly increased the mRNA level of *Ddb2* in diabetic mice (Fig. 7B), which probably contributed to the up-regulation of DDB2 protein expression (Fig. 7C). Immunofluorescence images revealed the co-localization of DDB2 and PAQR3 were significantly enhanced by GPS treatment in liver tissues under diabetic conditions (Fig. 7D). Co-IP results further confirmed that the combination of DDB2 and PAQR3 was reduced in diabetic mice, while GPS treatment promoted the interaction of DDB2 and PAQR3 in liver tissues of diabetic mice (Fig. 7E). We measured the ubiquitination level of PAQR3 in liver tissue; ubiquitination of PAQR3 was down-regulated during diabetes, which was accompanied by the up-regulation of PAQR3 protein (Fig. 7F). Results further indicate that GPS increased DDB2 expression, which probably promoted the ubiquitination and degradation of PAQR3 (Fig. 7F). Taken together, these results suggest that GPS

inhibited PAQR3 expression *via* DDB2-mediated PAQR3 ubiquitin-mediated degradation in diabetic mice.

4. Discussion

The liver plays a crucial role in the homeostasis of glucose and lipid in the body[47]. It is well recognized that a high-fat diet and sedentary lifestyle contributes to increase body fat deposition and thus to an increased risk to develop NAFLD as well as hepatic insulin resistance[48]. As the main active component of *Gentiana manshurica Kitagawa*, gentiopicroside has biological activity against a variety of liver diseases including ALD[34,49], cholestatic liver disease[50] and drug-induced liver injury[51,52]. Recently, GPS was found to play a role in alleviating diabetes and diabetic complications including retinal microvasculopathy and peripheral neuropathy[36,37]. Additionally, our previous study determined the hypoglycemic and renal protective effects of GPS[38]. However, there is still lack of systematic studies on the hypoglycemic and hypolipidemic effects of GPS in HFD-induced diabetes, and the potential mechanisms for improving diabetes remain unclear. In this study, we demonstrate that gentiopicroside protected mice from STZ−HFD-induced metabolic disorders, including hepatic insulin resistance, hepatic ectopic lipid deposition and hepatic steatosis. Mechanically, GPS promoted the interaction between PAQR3 and DDB2 to further induce DDB2-mediated PAQR3 ubiquitin degradation. Importantly, GPS directly bound to the N-terminus of PAQR3 to spatially inhibit the interaction between PAQR3 and P110α to restore the PI3K/AKT signaling pathway, thereby improving insulin resistance.

It is recognized that a high fat diet (HFD) combined with low-dose STZ injection is sufficient to cause insulin resistance and generate the pathological characteristics of type II diabetes[53]. *In vivo* results have shown HFD−STZ induction dramatically promotes lipid synthesis and ectopic deposition in liver and increased hepatic glycogen deposition, leading to hyperglycemia and hyperlipidemia. However, in our study abnormal glycolipid indicators, including FBG, GSP, TG, TC, and LDL-C, etc., were improved by GPS administration for 8 weeks. In addition, GPS increased hepatic glycogen storage and decreased lipid deposition in liver. It is established that metformin, the first-line treatment for type 2 diabetes, reduces hepatic glucose production by decreasing gluconeogenesis[54]. In this study, 100 mg/kg GPS was shown to possess an ameliorative effect comparable to that of 195 mg/kg metformin. As a proven anti-inflammatory and antioxidant natural product, GPS has been demonstrated to modulate the aberrant production of inflammatory molecular and endogenous antioxidants, and prevent renal fibrosis and alcoholic hepatosteatosis[34,38]. Here, we found that the up-regulation of the inflammatory adhesion molecules and fibrosis matrix was also inhibited, implying a protective role for GPS in hepatosteatosis induced by HFD.

Post-insulin receptor signaling obstruction is the main mechanism for insulin-resistant diabetes[8]. In the PI3K/AKT axis, PI3K is recruited to the insulin receptor by the insulin receptor substrate (IRS) protein under physiological conditions and activates the catalytic subunit p110α to catalyze the formation of PIP3, which then phosphorylates and activates AKT to combine with PDK[55]. In obesity, ectopic lipid deposition contributes to the obstruction of PI3K/AKT axis, which results in reduced glycogen synthesis/storage and a failure to suppress the release of glucose from the liver into the peripheral circulation[1]. Phosphoinositide 3-kinases are becoming an important emerging class of drug targets, and the mechanisms of PI3K activation are being defined[56]. As a proven anti-inflammatory natural product, GPS has been demonstrated to modulate lipid metabolism and promote cell survival in chemical-induced liver injury and ALD models[34,50]. In the present study, we found that GPS could not influence the mRNA levels of *INSR* and *IRS1*, and failed to restored INSR expression and IRS-1 phosphorylation. However, our results demonstrate that GPS promoted impaired PI3K (the phosphorylated forms at Tyr458), AKT (the phosphorylated forms at Ser473) and GSK3β (the phosphorylated forms at Tyr216) signaling *in vivo* and *in vitro*, thereby ameliorating hepatic insulin resistance to improve glycolipid metabolism. Notably, accumulating studies have highlighted the role of PAQR3 in modulating glucose and lipid metabolism. PAQR3 promotes cholesterol synthesis by anchoring the Scap/SREBP complex to the Golgi apparatus[57] and facilitating interaction between LDLR and PCSK9[27]. Furthermore, PAQR3 could initiate cell autophagy *via* the regulation of ATG14-linked class III PI3K activation upon glucose starvation[58]. Importantly, aberrant up-regulation of PAQR3 expression has been observed in the progression of diabetes, which negatively modulates insulin signaling by shunting class I PI3K p110α to the Golgi apparatus[28]. This has focused attention on PAQR3 as a novel target to modulate PI3K activity. Here, we found that GPS inhibited PAQR3 protein expression to reduce the interaction between PAQR3 and P110α, thereby facilitating the interaction between P110α and P85α to promote PI3K activation. Moreover, our results demonstrate that PAQR3 knockdown was sufficient to restore the PI3K/AKT axis, whereas co-treated with GPS did not produce an additional effect. Furthermore, the activation of PI3K/AKT axis induced by GPS was also reversed by PAQR3 overexpression. These results demonstrate that PAQR3 probably a specific pharmacological target for GPS.

Interestingly, our results showed that GPS did not change the mRNA level of *PAQR3*, while significantly reducing the level of PAQR3 protein, implying that the GPS-mediated down-regulation of PAQR3 expression was not transcriptionally dependent. It has been shown that PAQR3 is degraded by the ubiquitin−proteasome pathway, while the specific ubiquitination form of PAQR3 remains unclear[32]. Here, we clarified that PAQR3 could indeed be polyubiquitinated and was mainly modified by K48-linked polyubiquitination. Furthermore, we found that GPS strongly promoted PAQR3 ubiquitination, which probably contributes to PAQR3 protein degradation. Notably, DDB2, a substrate recognition protein together with DDB1 and CUL4A to form a ubiquitin ligase complex, has been identified as a post-translational regulator of PAQR3, which directly binds to PAQR3 to promote the ubiquitination of PAQR3[32]. We confirmed that DDB2 expression was down-regulated in PA-treated HepG2 cells and HFD-induced mice, which was accompanied by the down-regulation of PAQR3 ubiquitination. *DDB2* overexpression largely increased PAQR3 ubiquitination and promoted PAQR3 degradation, confirming the negative role of DDB2 in modulating PAQR3 protein expression. Importantly, we found that GPS increased the *DDB2* mRNA level to up-regulate DDB2 protein expression and facilitated the interaction between DDB2 and PAQR3. Knockdown of *DDB2* reversed the increased PAQR3 ubiquitination induced by GPS co-treatment, implying DDB2-mediated PAQR3 ubiquitin degradation contributed to the PAQR3 degradation induced by GPS treatment. *In vivo* results showed that GPS increased DDB2 expression and PAQR3 ubiquitination in HFD-induced mice, which might contribute to the degradation of PAQR3. Taken together, an important finding in

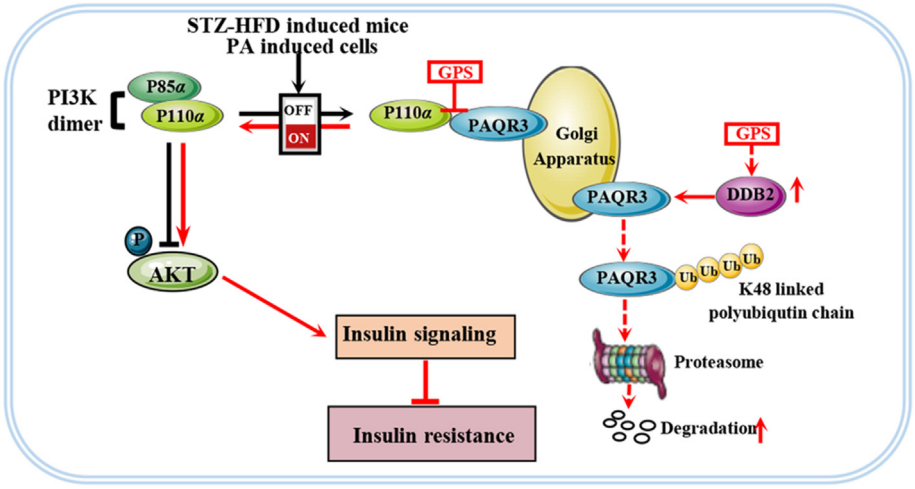

Figure 8 Graphic illustration of the mechanism of GPS in ameliorating insulin resistance. In diabetes, the up-regulated PAQR3 shunts cytosolic p110α to the Golgi apparatus while competing with p85α subunit in forming a PI3K complex with p110α, thereby negatively regulating insulin signaling. GPS treatment ameliorated high-fat diet (HFD) and palmitatic acid (PA)-induced hepatic insulin resistance by promoting PI3K/AKT axis activation. Mechanistically, on the one hand, GPS facilitated the interaction between DDB2 and PAQR3 to promote DDB2-mediated PAQR3 ubiquitin degradation, on the other hand, GPS directly bound to PAQR3 and spatially inhibited the interaction between PAQR3 and the PI3K catalytic subunit (P110α) to restore the PI3K/AKT signaling pathway.

this study is that GPS triggers PAQR3 Ub/proteasome-dependent degradation *via* the up-regulation of DDB2.

In vitro and *in vivo* evidence has been reported for a unique role of PAQR3 in the spatial regulation of PI3K *via* a capacity to sequester the p110α subunit to the Golgi apparatus, and further exploration found that the 71 NH_2-terminal amino acid residues of PAQR3 were sufficient to mediate the interaction with p110α[20,28]. Here, the SPR, MST and TSA assays confirmed that GPS directly interacted with PAQR3 proteins in a positive dose-dependent manner and the K_d value was 30−50 μmol/L. Furthermore, we established a homology model of PAQR3 (due to the lack of protein crystal structure), and molecular virtual docking results demonstrated that GPS could dock to the N-terminal pocket of PAQR3. GPS formed seven key hydrogen bonds with the N-terminus amino acids including Leu40, Asp42, Glu69, Tyr125 and Ser129 of PAQR3 to stabilize the binding conformation. Therefore, we conclude that GPS may cause steric hindrance in the N-terminal and prevent PAQR3 from anchoring P110α. In addition, we deleted Glu69, which had a strong intermolecular interaction with GPS, to identify the key binding site. The SPR and CETSA results showed that the capacity of GPS to bind with PAQR3 proteins was dramatically impaired by Glu69 deletion, implying Glu69 was critical for PAQR3 to bind to GPS. These results suggest that GPS functions as a PAQR3 inhibitor and is one of mechanisms by which GPS can ameliorate insulin resistance. Of note, myeloid-specific deletion of PAQR3 in mice may be needed to further validate the anti-insulin resistance effect of GPS *in vivo*. In addition, structural optimization of GPS to increase the affinity with PAQR3 will be carried out in further studies.

5. Conclusions

Our study elucidated a novel target of GPS in improving insulin resistance. We found that GPS diminished PAQR3 expression by promoting DDB2-mediated PAQR3 ubiquitin degradation. Importantly, we demonstrated that GPS bound directly to the N-terminus of PAQR3 and spatially inhibited the interaction between PAQR3 and P110α to restore the PI3K/AKT signaling pathway (Fig. 8A). Our findings provide a rationale for the potential application of GPS to restore insulin sensitivity in diabetes.

Acknowledgments

This work was supported by research grants from the National Natural Science Foundation of China (No. 81770816 and 81973375), the Key Project of Natural Science Foundation of Guangdong Province, China (No. 2017A030311036), Seed Program of Guangdong Province (No. 2017B090903004, China) and Guangdong Provincial Key Field and Program Project (No. 2020B1111100004, China).

Author contributions

Haiming Xiao designed and performed the study; Haiming Xiao and Xiaohong Sun wrote the manuscript; Zeyuan Lin analyzed the data; Meng Zhang and Zhanchi Xu contributed to language polishing. Peiqing Liu, Zhongqiu Liu and Heqing Huang conceived and supervised the study; and all authors have reviewed and approved the final version of the manuscript.

Conflicts of interest

The authors declare no conflicts of interest.

Appendix A. Supporting information

Supporting data to this article can be found online at https://doi.org/10.1016/j.apsb.2021.12.023.

References

1. Kahn SE, Hull RL, Utzschneider KM. Mechanisms linking obesity to insulin resistance and type 2 diabetes. *Nature* 2006;**444**:840−6.
2. Cho NH, Shaw JE, Karuranga S, Huang Y, Fernandes JDD, Ohlrogge AW, et al. IDF Diabetes Atlas: global estimates of diabetes prevalence for 2017 and projections for 2045. *Diabetes Res Clin Pract* 2018;**138**:271−81.
3. Saltiel AR, Kahn CR. Insulin signalling and the regulation of glucose and lipid metabolism. *Nature* 2001;**414**:799−806.
4. Choi K, Kim YB. Molecular mechanism of insulin resistance in obesity and type 2 diabetes. *Kor J Intern Med* 2010;**25**:119−29.
5. Engin A. Non-alcoholic fatty liver disease. *Adv Exp Med Biol* 2017; **960**:443−67.
6. Gastaldelli A, Cusi K. From NASH to diabetes and from diabetes to NASH: mechanisms and treatment options. *JHEP Rep* 2019;**1**:312−28.
7. Younossi ZM, Golabi P, de Avila L, Paik JM, Srishord M, Fukui N, et al. The global epidemiology of NAFLD and NASH in patients with type 2 diabetes: a systematic review and meta-analysis. *J Hepatol* 2019;**71**:793−801.
8. Cefalu WT, Berg EG, Saraco M, Petersen MP, Uelmen S, Robinson S, et al. Classification and diagnosis of diabetes: standards of medical care in diabetes-2019. *Diabetes Care* 2019;**42**:S13−28.
9. Wang X, Wang Z, Chen Y. The functions of PI3K/AKT signaling pathway in glucose homeostasis. *Chin Bull Life Sci* 2013;**25**:133−9.
10. Petersen MC, Shulman GI. Mechanisma of insulin action and insulin resistance. *Physiol Rev* 2018;**98**:2133−223.
11. Lee J, Kim MS. The role of GSK3 in glucose homeostasis and the development of insulin resistance. *Diabetes Res Clin Pract* 2007;**77**: S49−57.
12. Ni YG, Wang N, Cao DJ, Sachan N, Morris DJ, Gerard RD, et al. FoxO transcription factors activate Akt and attenuate insulin signaling in heart by inhibiting protein phosphatasesy. *Proc Natl Acad Sci U S A* 2007;**104**:20517−22.
13. Li X, Li Y, Yang W, Xiao C, Fu S, Deng Q, et al. SREBP-1c overexpression induces triglycerides accumulation through increasing lipid synthesis and decreasing lipid oxidation and VLDL assembly in bovine hepatocytes. *J Steroid Biochem Mol Biol* 2014;**143**:174−82.
14. Plum L, Rother E, Muenzberg H, Wunderlich FT, Morgan DA, Hampel B, et al. Enhanced leptin-stimulated PI3K activation in the CNS promotes white adipose tissue transdifferentiation. *Cell Metabol* 2007;**6**:431−45.
15. Liu TY, Shi CX, Gao R, Sun HJ, Xiong XQ, Ding L, et al. Irisin inhibits hepatic gluconeogenesis and increases glycogen synthesis *via* the PI3K/Akt pathway in type 2 diabetic mice and hepatocytes. *Clin Sci (Lond)* 2015;**129**:839−50.
16. Marone R, Cmijanovic V, Giese B, Wymann MP. Targeting phosphoinositide 3-kinase—moving towards therapy. *Biochim Biophys Acta* 2008;**1784**:159−85.
17. Knight ZA, Gonzalez B, Feldman ME, Zunder ER, Goldenberg DD, Williams O, et al. A pharmacological map of the PI3-K family defines a role for p110 alpha in insulin signaling. *Cell* 2006;**125**:733−47.
18. Vanhaesebroeck B, Guillermet-Guibert J, Graupera M, Bilanges B. The emerging mechanisms of isoform-specific PI3K signalling. *Nat Rev Mol Cell Biol* 2010;**11**:329−41.
19. Taniguchi CM, Tran TT, Kondo T, Luo J, Ueki K, Cantley LC, et al. Phosphoinositide 3-kinase regulatory subunit p85 alpha suppresses insulin action *via* positive regulation of PTEN. *Proc Natl Acad Sci U S A* 2006;**103**:12093−7.
20. Feng L, Xie XD, Ding QR, Luo XL, He J, Fan FJ, et al. Spatial regulation of Raf kinase signaling by RKTG. *Proc Natl Acad Sci U S A* 2007;**104**:14348−53.
21. Yu X, Li Z, Chan MTV, Wu WKK. PAQR3: a novel tumor suppressor gene. *Am J Cancer Res* 2015;**5**:2562−8.
22. Lei L, Ling ZN, Chen XL, Hong LL, Ling ZQ. Characterization of the Golgi scaffold protein PAQR3, and its role in tumor suppression and metabolic pathway compartmentalization. *Cancer Manag Res* 2020; **12**:353−62.
23. Chen L, Sun X, Xiao H, Xu F, Yang Y, Lin Z, et al. PAQR3 regulates phosphorylation of FoxO1 in insulin-resistant HepG2 cells *via* NF-kappa B signaling pathway. *Exp Cell Res* 2019;**381**:301−10.
24. Zou Y, Chen Z, Li J, Gong W, Zhang L, Xu F, et al. Progestin and AdipoQ receptor 3 upregulates fibronectin and intercellular adhesion molecule-1 in glomerular mesangial cells *via* activating NF-κB signaling pathway under high glucose conditions. *Front Endocrinol (Lausanne)* 2018;**9**:275.
25. Wang LD, Wang X, Li ZH, Xia TT, Zhu L, Liu B, et al. PAQR3 has modulatory roles in obesity, energy metabolism, and leptin signaling. *Endocrinology* 2013;**154**:4525−35.
26. Zhao ZL, Xu DQ, Wang Z, Wang L, Han RM, Wang ZZ, et al. Hepatic PPAR function is controlled by polyubiquitination and proteasome-mediated degradation through the coordinated actions of PAQR3 and HUWE1. *Hepatology* 2018;**68**:289−303.
27. Huang MQ, Zhao ZL, Cao QQ, You X, Wei SY, Zhao JY, et al. PAQR3 modulates blood cholesterol level by facilitating interaction between LDLR and PCSK9. *Metabolism* 2019;**94**:88−95.
28. Wang X, Wang LD, Zhu L, Pan Y, Xiao F, Liu WZ, et al. PAQR3 modulates insulin signaling by shunting phosphoinositide 3-kinase p110 alpha to the Golgi apparatus. *Diabetes* 2013;**62**:444−56.
29. Stoyanova T, Roy N, Kopanja D, Bagchi S, Raychaudhuri P. DDB2 decides cell fate following DNA damage. *Proc Natl Acad Sci U S A* 2009;**106**:10690−5.
30. Yan YY, Zhang XS, Legerski RJ. Artemis interacts with the Cul4A-DDB1 (DDB2) ubiquitin E3 ligase and regulates degradation of the CDK inhibitor p27. *Cell Cycle* 2011;**10**:4098−109.
31. Lai TC, Hu MC. Regulation of liver receptor homologue-1 by DDB2 E3 ligase activity is critical for hepatic glucose metabolism. *Sci Rep* 2019;**9**:5304.
32. Qiao SS, Guo WW, Liao LJ, Wang L, Wang Z, Zhang R, et al. DDB2 is involved in ubiquitination and degradation of PAQR3 and regulates tumorigenesis of gastric cancer cells. *Biochem J* 2015;**469**:469−80.
33. Wu S, Ning Y, Zhao Y, Sun W, Thorimbert S, Dechoux L, et al. Research progress of natural product gentiopicroside—a secoiridoid compound. *Mini Rev Med Chem* 2017;**17**:62−77.
34. Li X, Zhang Y, Jin Q, Xia KL, Jiang M, Cui BW, et al. Liver kinase B1/AMP-activated protein kinase-mediated regulation by gentiopicroside ameliorates P2X7 receptor-dependent alcoholic hepatosteatosis. *Br J Pharmacol* 2018;**175**:1451−70.
35. Jin MY, Feng HH, Wang Y, Yan SR, Shen BY, Li Z, et al. Gentiopicroside ameliorates oxidative stress and lipid accumulation through nuclear factor erythroid 2-related factor 2 activation. *Oxid Med Cell Longev* 2020;**2020**:13.
36. Lu Y, Yao J, Gong C, Wang B, Zhou P, Zhou S, et al. Gentiopicroside ameliorates diabetic peripheral neuropathy by modulating PPAR-Gamma/AMPK/ACC signaling pathway. *Cell Physiol Biochem* 2018;**50**:585−96.
37. Zhang X, Shi E, Yang L, Fu W, Hu F, Zhou X. Gentiopicroside attenuates diabetic retinopathy by inhibiting inflammation, oxidative stress, and NF-kappa B activation in rat model. *Eur J Inflamm* 2019; **17**: 205873921984783.
38. Xiao H, Sun X, Liu R, Chen Z, Lin Z, Yang Y, et al. Gentiopicroside activates the bile acid receptor Gpbar1 (TGR5) to repress NF-kappaB pathway and ameliorate diabetic nephropathy. *Pharmacol Res* 2020; **151**:104559.
39. Chen Z, Sun X, Chen Q, Lan T, Huang K, Xiao H, et al. Connexin32 ameliorates renal fibrosis in diabetic mice by promoting K48-linked NADPH oxidase 4 polyubiquitination and degradation. *Br J Pharmacol* 2020;**177**:145−60.
40. Han CC, Li YF, Zhang YW, Wang Y, Cui DQ, Luo TT, et al. Targeted inhibition of GRK2 kinase domain by CP-25 to reverse fibroblast-like synoviocytes dysfunction and improve collagen-induced arthritis in rats. *Acta Pharm Sin B* 2021;**11**:1835−52.

41. Dziekan JM, Yu H, Chen D, Dai L, Wirjanata G, Larsson A, et al. Identifying purine nucleoside phosphorylase as the target of quinine using cellular thermal shift assay. *Sci Transl Med* 2019;**11**:473.
42. Gastaldelli A, Gaggini M, DeFronzo RA. Role of adipose tissue insulin resistance in the natural history of type 2 diabetes: results from the San Antonio metabolism study. *Diabetes* 2017;**66**:815−22.
43. Posey KA, Clegg DJ, Printz RL, Byun J, Morton GJ, Vivekanandan-Giri A, et al. Hypothalamic proinflammatory lipid accumulation, inflammation, and insulin resistance in rats fed a high-fat diet. *Am J Physiol Endocrinol Metab* 2009;**296**:E1003−12.
44. Gao D, Nong S, Huang X, Lu Y, Zhao H, Lin Y, et al. The effects of palmitate on hepatic insulin resistance are mediated by NADPH oxidase 3-derived reactive oxygen species through JNK and p38 (MAPK) pathways. *J Biol Chem* 2010;**285**:29965−73.
45. Li JY, Wang QE, Zhu QZ, El-Mahdy MA, Wani G, Praetorius-Ibba M, et al. DNA damage binding protein component DDB1 participates in nucleotide excision repair through DDB2 DNA-binding and cullin 4A ubiquitin ligase activity. *Cancer Res* 2006;**66**:8590−7.
46. Hoehn KL, Salmon AB, Hohnen-Behrens C, Turner N, Hoy AJ, Maghzal GJ, et al. Insulin resistance is a cellular antioxidant defense mechanism. *Proc Natl Acad Sci U S A* 2009;**106**:17787−92.
47. Gastaldelli A, Stefan N, Haering HU. Liver-targeting drugs and their effect on blood glucose and hepatic lipids. *Diabetologia* 2021;**64**:1461−79.
48. Friedman SL, Neuschwander-Tetri BA, Rinella M, Sanyal AJ. Mechanisms of NAFLD development and therapeutic strategies. *Nat Med* 2018;**24**:908−22.
49. Yang HX, Shang Y, Jin Q, Wu YL, Liu J, Qiao CY, et al. Gentiopicroside ameliorates the progression from hepatic steatosis to fibrosis induced by chronic alcohol intake. *Biomol Ther (Seoul)* 2020;**28**:320−7.
50. Tang XW, Yang QL, Yang F, Gong JT, Han H, Yang L, et al. Target profiling analyses of bile acids in the evaluation of hepatoprotective effect of gentiopicroside on ANIT-induced cholestatic liver injury in mice. *J Ethnopharmacol* 2016;**194**:63−71.
51. Dai K, Yi XJ, Huang XJ, Muhammad A, Li M, Li J, et al. Hepatoprotective activity of iridoids, seco-iridoids and analog glycosides from gentianaceae on HepG2 cells *via* CYP3A4 induction and mitochondrial pathway. *Food Funct* 2018;**9**:2673−83.
52. Han H, Xu L, Xiong K, Zhang T, Wang Z. Exploration of hepatoprotective effect of gentiopicroside on alpha-naphthylisothiocyanate-induced cholestatic liver injury in rats by comprehensive proteomic and metabolomic signatures. *Cell Physiol Biochem* 2018;**49**:1304−19.
53. Srinivasan K, Viswanad B, Asrat L, Kaul CL, Ramarao P. Combination of high-fat diet-fed and low-dose streptozotocin-treated rat: a model for type 2 diabetes and pharmacological screening. *Pharmacol Res* 2005;**52**:313−20.
54. Madiraju AK, Erion DM, Rahimi Y, Zhang XM, Braddock DT, Albright RA, et al. Metformin suppresses gluconeogenesis by inhibiting mitochondrial glycerophosphate dehydrogenase. *Nature* 2014;**510**:542−6.
55. Huang XJ, Liu GH, Guo J, Su ZQ. The PI3K/AKT pathway in obesity and type 2 diabetes. *Int J Biol Sci* 2018;**14**:1483−96.
56. Vanhaesebroeck B, Whitehead MA, Pineiro R. Molecules in medicine mini-review: isoforms of PI3K in biology and disease. *J Mol Med (Berl)* 2016;**94**:5−11.
57. Xu D, Wang Z, Zhang Y, Jiang W, Pan Y, Song BL, Chen Y. PAQR3 modulates cholesterol homeostasis by anchoring Scap/SREBP complex to the Golgi apparatus. *Nat Commun* 2015;**6**:8100.
58. Xu DQ, Wang Z, Wang CY, Zhang DY, Wan HD, Zhao ZL, et al. PAQR3 controls autophagy by integrating AMPK signaling to enhance ATG14L-associated PI3K activity. *EMBO J* 2016;**35**:496−514.